Title: The equilibrium theory of biodiversity dynamics: a general framework for scaling species richness and community abundance along environmental gradients

Running head: Theory of biodiversity dynamics

Article type: Major article

Authors: Jordan G. Okie[1]*, David Storch[2,3]

The authors wish to be identified to the reviewers.

Affiliations:

[1]School of Earth and Space Exploration, Arizona State University, Tempe, USA.

[2]Center for Theoretical Study, Charles University and the Czech Academy of Science, Prague, Czech Republic.

[3]Department of Ecology, Faculty of Science, Charles University, Prague, Czech Republic.

*Jordan.Okie@asu.edu

Teaser: Theory explaining macroecological biodiversity patterns through the effects of extinction, speciation, resource levels and the effect of biodiversity on community abundance

Keywords: speciation, extinction, ecological limits, latitudinal diversity gradient, community size; source pool; biodiversity-ecosystem function relationship.

Elements of paper: Abstract**,** Introduction, Results, Discussion, Materials and Methods, 5 main text figures, 2 main text table, 2 boxes, supplemental text, 2 supplemental figures, 3 supplemental tables.

Main text length (excluding references): 8,567 words.

Abstract

Large-scale temporal and spatial biodiversity patterns have traditionally been explained by multitudinous particular factors and a few theories. However, these theories lack sufficient generality and do not address fundamental interrelationships and coupled dynamics between resource availability, community abundance, and species richness. We propose the equilibrium theory of biodiversity dynamics (ETBD) to address these linkages. According to ETBD, equilibrium levels of species richness and community abundance emerge due to the population size-dependence of speciation and/or extinction rates, modulated by resource availability and the species-abundance distribution. In contrast to other theories, ETBD includes the effect of biodiversity on community abundance (BECA) and thus addresses phenomena such as niche complementarity, facilitation, and ecosystem engineering. It reveals how alternative stable states in both diversity and community abundance emerge from nonlinear BECA. ETBD predicts how the strength of BECA affects scaling relationships between species richness, (meta)community abundance, and resource availability along different environmental gradients. Using data on global-scale variation in tree species richness, we show how the general framework is useful for clarifying the role of speciation, extinction and resource availability in driving patterns in biodiversity and community abundance, such as the latitudinal diversity gradient.

Introduction

The biodiversity, abundance and biomass of living systems vary extraordinarily across the biosphere, through Earth history, and among major phyla. Understanding this large-scale variation and its consequences for the functioning and resilience of ecological systems is crucial for advancing ecological theory and forecasting the future of biodiversity and ecosystems in the Anthropocene (McGill 2019; Storch et al. 2022). Given the elevated extinctions underway in the Anthropocene, identifying the causes of global-scale patterns of species richness, community abundance and biomass is of particular importance.

The underlying causes for even the most well-studied patterns still remain hotly contested (Pontarp et al. 2019). The pattern of decrease in the number of species from the equator to the poles, documented in nearly all major taxa of multicellular eukaryotes, is one prominent example. Dozens of hypotheses have been formulated (Fine 2015), but no clear consensus has emerged. This lack of consensus is in part due to the multitudinous factors at play but also due to the lack of general theoretical frameworks to test hypotheses and disentangle large-scale diversity drivers. Recently, evidence is accumulating that large-scale spatial diversity patterns tend to converge onto similar relationships with resource availability and climatic variables regardless of differences in diversification histories (Field et al. 2009; Hawkins et al. 2012; Rabosky 2022), and the origination and extinction rates underlying diversity dynamics exhibit a dependence on diversity (Rabosky 2009; Rineau et al. 2022). These findings have been interpreted as evidence of the role of region or biome-specific ecological limits to species richness (Rabosky and Hurlbert 2015; Etienne et al. 2019), but the nature of these limits has not been entirely clear.

We've argued that such limits should be understood as stable equilibria of diversity dynamics that emerge from the links between macroevolutionary dynamics of speciation and extinction modulated by resource availability and community assembly, and that such equilibria

shape large-scale spatial and temporal patterns of diversity (Storch and Okie 2019). General theories of biodiversity dynamics (MacArthur and Wilson 1967; Hubbell 2001; Worm and Tittensor 2018) predict the existence of such biodiversity equilibria but suffer from some key shortcomings preventing them from providing a general framework to understanding diversity dynamics. First, they make overly stringent and unrealistic assumptions about the involved processes. For example, the neutral theory of biodiversity, besides assuming ecological equivalence among species that includes equal access to all resources, implicitly assumes that per-species speciation rate increases linearly with population size (Allen and Savage 2007) despite theoretical evidence that speciation rate can exhibit more complex dependencies on species abundance (Gavrilets 2003).

Second, most crucially, while these theories often address (implicitly or explicitly) how community abundance (total biomass or number of individuals) limits species richness by influencing rates of extinction and origination (e.g., Hubbell 2001; Allen and Savage 2007), they take community abundance as an external parameter or static variable and do not address the possibility that the size of the community may itself be a dynamical variable that depends both on the environment and the realized species richness of the community. This is highly problematic since the number of species in a community tends to positively affect the total amount of resources used and converted into community abundance (Loreau 1998; Nijs and Roy 2000; Tilman et al. 2001; Cardinale et al. 2006), as shown in experimental studies of the biodiversity-ecosystem function relationship (Bell et al. 2005; Cardinale et al. 2006; O'Connor et al. 2017), suggested by macroecological and paleobiological analyses (e.g., Grace et al. 2016; Liang et al. 2016*a*), and demonstrated with theoretical models (Loreau 1998; Liang et al. 2015; Harte et al. 2022). We hereby refer to this effect as the biodiversity effect on community abundance or BECA.

We contend that there is a need for theory that addresses the coupled dynamics of species richness and community abundance. Such coupled dynamics may have non-trivial consequences for

88 biodiversity patterns. The bidirectional interactions between biodiversity and community
89 abundance could lead to an emergence of multiple equilibria and alter how equilibria respond to
90 changing conditions and environmental gradients. These effects could shape temporal and
91 geographic patterns of biodiversity and biomass, as well as their response to environmental
92 perturbations.

93 Here we provide the first formal presentation of the Equilibrium Theory of Biodiversity
94 Dynamics and present a new quantitative framework for understanding changes in species richness
95 and community abundance along environmental gradients. We build on and substantially add to
96 previous work in which we first described the bones of ETBD (Storch et al. 2018, 2022; Storch and
97 Okie 2019). The new framework predicts the scaling relationships between equilibria of biodiversity
98 and community abundance and their variation along gradients in extinction, speciation, and
99 resource availability, addressing (but not assuming) the possibility that species diversity may
100 influence resource consumption and community abundance. The theory also addresses the role of
101 the species abundance distribution and of the population size-dependence of extinction and
102 speciation in modulating the equilibria. It demonstrates how alternative equilibria in biodiversity
103 and community abundance naturally emerge from few assumptions. To illustrate the framework's
104 application, we apply it to global-scale variation in tree diversity, shedding light on the
105 underpinnings of the latitudinal diversity gradient in trees.
106
107 **Results**
108 ETBD focuses on the dynamics of biodiversity at the scales at which variation in speciation rate
109 outweighs colonization rate in its contribution to biodiversity dynamics. ETBD thus addresses the
110 species richness of biomes or biogeographic provinces (sensu Rosenzweig 1995) . It considers the
111 species richness and community abundance of biomes to be independently determined by the

drivers of biodiversity dynamics such that biomes are assumed to not be samples of each other. Here we use the word *community* to refer to the assemblage of species in these large-scale areas.

Universal Emergence of Diversity Equilibria

The central assumption of ETBD is that a population's probability of extinction and/or speciation exhibit some level of dependence on population size. There is a solid empirical and theoretical basis for this assumption, in particular that extinction probability is generally negatively dependent on population size (e.g., Pimm et al. 1988; McDonald and Brown 1992; Rosenzweig 1995; Griffen and Drake 2008; Okie and Brown 2009; Ovaskainen and Meerson 2010). A consequence of this assumption is that for communities that aren't on their way to extinction, the curve quantifying the population-size (*N*) dependence of extinction must necessarily intersect the curve quantifying the N-dependence of speciation. The reason is that the origination rate cannot be higher than the extinction rate over all values of *N*, since as *N* approaches 0, extinction probability necessarily approaches 1 whereas speciation probability approaches zero. Consequently, at this universal intersection, the (negative) slope of the extinction curves must always be lower than the slope of the speciation curve (Figure 1A).

This intersection of curves indicates a population size at which per species origination and extinction rates are equal. This intersection, along with the species abundance distribution, determine the mean species abundance at which a community's total speciation rate is equal to total extinction rate, which we call the equilibrium mean abundance $\widehat{N}$. If all species in the community had the same abundance, then $\widehat{N}$ would be exactly equal to the intersection of the speciation and extinction curves. If, instead, species vary in their abundance, then $\widehat{N}$ deviates from the intersection, but we have found that it is still set by the intersection (see below and SOM) and remains uniquely determined by the species-abundance distribution (SAD). Consequently, in a plot

of species richness *S* against community abundance *J* on the vertical axis, there is a straight diagonal line called the S-nullcline that has a slope equal to mean equilibrium population size $\widehat{N}$ (since the slope is equal to *J*/*S*, which is the mean population size) and represents communities in which total speciation rate is equal to total extinction rate (i.e., dS/dt = 0; Fig 1B, see Supplementary Materials for mathematical details). The equation for this S-nullcline is $J = \widehat{N}S$. A linear S-nullcline thus reflects the baseline scenario of biodiversity dynamics in which the parameters of extinction probability, speciation probability, and the species abundance distribution are not directly affected by diversity or community abundance.

Because the negative slope of the extinction curve is lower than the slope of the origination curve, this nullcline exhibits *attractor* dynamics in which communities perturbed out of equilibrium return back to the S-nullcline, which we thus call an *attractor* S-nullcline. The reason is that points to the right of this S-nullcline represent communities where mean population size (i.e., *J*/*S*) is lower than $\widehat{N}$ (and thus extinction is generally higher than speciation rate), and vice versa.

Addressing the Biodiversity Effect on Community Abundance

Since all points along the S-nullcline represent potential biodiversity equilibria, a community's equilibrium point along its S-nullcline is determined by its community abundance *J.* In contrast to other theories of biodiversity dynamics that typically assume that *J* is constant for a community or metacommunity (e.g. Hubbell 2001), ETBD assumes that *J* may itself be influenced by *S.* The rationale for this assumption lies in the realization that *J* is not a feature directly determined by the environment, but instead it is driven by the interplay of population dynamics of all involved species. While in some specific cases *J* may be independent of *S,* it is reasonable to assume an addition of species often leads to the utilization of previously unused resources, and thus S has a positive effect on *J*. Consequently, the J-nullcline, the line delineating the values of *S* and *J* for which *J* can be in

equilibrium (i.e., for which d*J*/d*t* = 0), is an increasing function of *S* (Fig 1B thick red line), up to a maximum *J* determined by the maximum energy available to the system divided by mean individual metabolic rate (thin red line, see Fig. 1B). A community thus has an equilibrium point for *S* and *J* ($[\hat{S}, \hat{J}]$) located at the intersection of the S-nullcline and J-nullcline.

Whereas theoretical and empirical understanding of the overall shape of the J-nullcline is limited, there are general quantitative features of the J-nullcline that have implications for biodiversity equilibria. All-else-being equal, greater total energy availability increases the total number of individuals that a community of a given *S* can support (Fig. 1C, top). Consider also that the shape of the J-nullcline reflects the balance of ecological factors governing the slope of the J-nullcline at a given *S* and the degree to which these factors change or not with *S*. At a given *S*, the slope β of the line tangent to the J-nullcline in log-log space—that is, $\beta = d[log(J)]/d[log(S)]$—quantifies the aggregate effects of increasing species richness on the consumption and conversion of resources into abundance (Fig. 2). We consider three general, fundamental scenarios. (1) Facilitation and ecosystem engineering ($\beta > 1$): When positive effects of diversity on resource use dominate, each addition of a species increases, on average, the mean abundance at which $\mathrm{dJ/dt} = 0$, leading to an upward-acceleration in the J-nullcline. (2) Ideal complementarity ($\beta = 1$): When each additional species is, on average, able to use a whole new set of resources just as effectively as the present species and without taking resources away from the present species, the J-nullcline follows a straight line. (3) Competition with some level of niche complementarity ($0 < \beta < 1$) or no niche complementarity, i.e. complete niche overlap ($\beta = 0$): If each additional species converts fewer unused resources into abundance than the present species, then the J-nullcline exhibits decelerating behavior. This behavior may have several reasons, including niche overlap or a need to specialize due to increasing competition, and is expected when the community approaches

183 energetic limits of the environment, i.e. the upper ceiling to community abundance. In general,
184 values of β close to zero indicate more intense competition for resources.

185 In Figure 1C (bottom), we show the potential scenario in which facilitation dominates the J-
186 nullcline scaling behavior at low *S* and competition dominates the behavior at high *S*, leading to a
187 sigmoidal J-nullcline. Such facilitation at low *S* may be prevalent in physically harsh environments,
188 deserts, certain microbial communities (Morris et al. 2013), and other ecological systems reliant on
189 syntrophy or ecosystem engineering (Jones et al. 1997), as primary succession is known to be driven
190 by facilitation (Connell and Slatyer 1977; Cardinale et al. 2002; Walker and Del Moral 2003; Kjær et
191 al. 2018; Castillo et al. 2021). However, for most environmental gradients of high-diversity
192 contemporary communities, we expect that at large scales communities fall within a phase of the J-
193 nullcline in which β is positive and less than one, (O'Connor et al. 2017).

194

195 *Stability and Emergence of Multiple Equilibria*

196 Having shown how equilibria emerge from the intersection of S and J-nullclines and the eco-
197 evolutionary underpinnings of the nullclines, it is necessary to elucidate the nature of the equilibria
198 – whether they are stable or unstable. The stability of the equilibrium point $[\hat{S}, \hat{J}]$ emerges from the
199 interaction of the *S* and J-nullclines. The stability follows some basic rules due to differences in the
200 timescales of births and deaths versus speciation and extinction, circumventing the need for
201 stability analysis of a specific system of differential equations. When communities are perturbed
202 from the J-nullcline, the absolute rate of change in community abundance is much higher than the
203 absolute rate of change in species richness, due to the difference between ecological and
204 evolutionary time comprising population change versus speciation/extinction, respectively.
205 Consequently, these non-equilibrium communities follow near-vertical vectors (trajectories) until

206 they converge on the J-nullcline, at which point their path traces the J-nullcline in the direction
207 determined by their position relative to S-nullcline and the character of the S-nullclines (Figure 1B).
208 Because the universal attractor S-nullcline exhibits attractor dynamics, if the J-nullcline is
209 less steep than the attractor S-nullcline around their intersection point, exhibiting $\beta < 1$, then the
210 equilibrium is stable (Figure 1B). A perturbed community with $S < \hat{S}$ follow trajectories that
211 converge on the J-nullcline and then, since the J-nullcline is higher than the S-nullcline at S < $\hat{S}$, the
212 community proceeds along the J-nullcline towards the equilibrium point. In contrast, if $\beta > 1$ in the
213 vicinity of the equilibrium point, then the equilibrium point is unstable (Figure 1C, bottom; see also
214 Box 1). However, due to energetic limits to *J*, *J* cannot increase indefinitely as $\beta > 1$; eventually, at
215 very high *J*, the J-nullcline necessarily must flatten out, leading to the J-nullcline exhibiting $\beta < 1$ at
216 an upper equilibrium point.
217 In addition to this universal stable equilibrium point, additional lower stable equilibria may
218 emerge in a variety of scenarios. For instance, the speciation and extinction curves could have a
219 second intersection point, due to P_V being hump-shaped or P_x being U-shaped (e.g. if large
220 populations have high extinction probabilities due to their susceptibility to epidemics). This second
221 intersection point can lead to a second S-nullcline that exhibits repulsive rather than attractor
222 dynamics (see Box 1 for details). If the J-nullcline is sigmoidal, this can lead to an additional stable
223 equilibrium at low S (where facilitation dominates) and an additional tipping point (Box 1).
224
225 *Scaling Relationships for Gradients in Energy, Speciation, and Extinction*
226 ETBD highlights that there are three fundamental drivers of biodiversity equilibria: energy
227 availability, the extinction-speciation balance, and the shape of the J-nullcline (Figure 1C). We thus
228 first address how equilibrium *S* and *J* should change as a consequence of each of these three

fundamental drivers, and then present quantitative predictions for complex gradients in which more than one of these drivers are varying simultaneously.

The ETDB framework reveals that the scaling behavior of the J-nullcline, as quantified by β, fundamentally affects the scaling relationships between $\hat{S}$, $\hat{J}$, and *E*/*B*. Over a given range of *S*, the J-nullcline can be mathematized as a power-law function of *S* (e.g., Liang et al. 2016*a*), giving

$$\hat{J} = (\frac{E}{B})cS^{\beta}, \quad (1)$$

where *c* sets the fraction of the maximum available energy *E* used by a one-species community and $cS^{\beta} \leq 1$, reflecting the physical constraint that $J \geq S$. A thermodynamic constraint to Equation 1 is that *J* cannot be greater than maximum community abundance J_{max}, determined by the maximum available energy *E* divided by average individual metabolic rate *B*. Equation 1 makes the baseline assumption that changes in maximum available energy *E* or J_{max} have a positive linear effect on the "height" (intercept) of the J-nullcline.

Combining equation 1 with the equation for the linear S-nullcline, we obtain predictions for how *S* and *J* should change along a gradient in J_{max} *, E, or B,* which is a gradient in which only the position of the J-nullcline is changing:

$$\hat{S} \propto (E/B)^{1/(1-\beta)}, \quad (2)$$

$$\hat{J} \propto (E/B)^{1/(1-\beta)}, \quad (3)$$

and

$$\hat{S} \propto \hat{J}^{1}, \quad (4)$$

Thus, along gradients in resource availability, $\hat{S}$ is expected to scale linearly with $\hat{J}$. In contrast, along a speciation/extinction gradient, which is a gradient in which the S-nullcline is changing, we obtain:

$$\hat{S} \propto \hat{J}^{1/\beta} \quad (5)$$

Equations 2, 3, and 5 show that the BECA shapes the scaling of $\hat{S}$, $\hat{J}$, and *E*/*B*. For example, when competition with niche complementarity govern the BECA ($0 < \beta < 1$), Fig. 2), *S* and *J* increase

253 superlinearly (disproportionately) with *E*/*B* and $\hat{S}$ scales superlinearly with $\hat{J}$ along
254 speciation/extinction gradients. In contrast, when facilitation dominates ($\beta > 1$), *S* and $\hat{J}$ decrease
255 with *E*/*B*, because with facilitation, even fewer species are required to obtain a given community
256 abundance and equilibrium mean abundance. This finding can be graphically ascertained by
257 observing that intersection of the *S* and *J*-nullclines shifts downward and leftward when the height
258 of the J-nullcline increases due to increasing *E*/*B (*Figure S2*).* Note, however, that this equilibrium
259 point is only stable if it reflects the intersection of the J-nullcline with a second S-nullcline, which
260 occurs when the curves quantifying the population size-dependence of extinction and speciation
261 intersect twice (Box 1).

262 Equations 2-5 predict that in log-log plots of *S*, *J*, and *E*, straight lines are expected with
263 slopes equal to the exponents in the equations. These equations can be taken as the most general,
264 baseline predictions available in the absence of knowledge indicating changes in β. Indeed, a power
265 law model for the BECA relationship has empirical support from studies of the effect of diversity on
266 community biomass production, standing biomass, and resource consumption (Reich et al. 2012;
267 Liang et al. 2016*a*; O'Connor et al. 2017) and some theoretical basis (Mora et al. 2014; Harte et al.
268 2022), with β averaging around 0.26 across a variety of taxa and ecosystems (O'Connor et al. 2017).

269 We further develop the framework to quantify complex gradients along which both
270 speciation/extinction and *E*/*B* vary, which can be used to disentangle the relative contributions of
271 variation in speciation/extinction versus *E*/*B*. Consider the most general, coarse-grained approach:
272 both *E*/*B* and the speciation/extinction balance (i.e., equilibrium mean abundance $\widehat{N}$) are associated
273 with some environmental variable G as either power functions or exponential functions, such that

274 $$E/B = r_0 G^{r_1} \text{ or } E/B = r_0 e^{r_1 G} \quad (6)$$

275 and

276 $$\widehat{N} = g_0 G^{g_1} \text{ or } \widehat{N} = g_0 e^{g_1 G}, \quad (7)$$

where r_0 and g_0 are normalization coefficients and r_1 and g_1 are scaling exponents quantifying the effects of G. The choice of whether to consider the power or exponential functions to quantify a particular gradient should be made based on theoretical or practical reasons. For instance, typically, researchers consider species richness to vary exponentially with temperature and latitude (Currie et al. 2004; Storch 2012), both because temperature has an exponential effect on biological rates (Brown et al. 2004) and because scatterplots of log richness versus temperature and latitude tend to minimize statistical heteroscedasticity compared to log-log or untransformed plots of these variables.

Along a purely resource-driven gradient, equilibrium mean abundance doesn't vary and so $g_1 = 0$. Along a purely speciation/extinction-driven gradient, resource availability doesn't vary and so $r_1 = 0$. When $\frac{g_1}{r_1} < 0$, the two drivers (the positive effects of the speciation/extinction balance and resource availability on diversity) are concordant along the gradient, leading to what we call a *concordance gradient*. When $\frac{g_1}{r_1} > 0$, the effects are discordant such that at higher resource availability, speciation is lower or extinction is higher, leading to a *discordance gradient.* In a perfectly discordant gradient, the drivers of diversity vary completely opposingly, leading to $\frac{g_1}{r_1} = 1$ and no change in diversity along the gradient.

The resulting scaling predictions for these gradients are:

$$\hat{S} \propto (E/B)^{Q_{SE}}, \quad (8)$$

$$\hat{J} \propto (E/B)^{Q_{JE}}, \quad (9)$$

$$\hat{S} \propto \hat{J}^{Q_{SJ}}, \quad (10)$$

$$\hat{S} \propto G^{(r_1 - g_1)/(1-\beta)} \text{ or } \hat{S} \propto e^{\frac{(r_1 - g_1)}{(1-\beta)}G} \quad (11)$$

and

$$\hat{J} \propto G^{(r_1 - g_1\beta)/(1-\beta)} \text{ or } \hat{J} \propto e^{\frac{(r_1 - g_1\beta)}{(1-\beta)}G} \quad (12)$$

Where $Q_{SE} = (1 - g_1/r_1)/(1 - \beta)$, $Q_{JE} = (1 - g_1\beta/r_1)/(1 - \beta)$, and $Q_{SJ} = (1 - g_1/r_1)/(1 - g_1\beta/r_1)$ and the formulas for Equations 11 and 12 depend on whether the gradient variable is assumed to have a power law effect (first formula) or exponential effect (second formula) on $\widehat{N}$ and E/B. Figure 2 and Equations 8-12 show that the scaling of $\hat{S}$, $\hat{J}$, and *E* depends only on β and the ratio g_1/r_1. For example, when $\beta < 1$, $\hat{S}$ only increases with *E*/*B* if $g_1/r_1 < 1$; that is, as long as the gradient isn't strongly discordant. Along a discordance gradient, a great variety of *S*-*J* relationships can occur, depending on β and whether or not the speciation/extinction balance versus *E*/*B* is varying most along the gradient (Fig. 3). In a perfectly discordant gradient, although no change in biodiversity along the gradient occurs, there is a change in *J* along the gradient that is determined by β. Similarly to a resource gradient, along concordance gradients, β values higher than 1 can lead to negative *S*-*E* and *J*-*E* relationships, but only in the presence of a second S-nullcline. Species richness and abundance patterns along environmental/geographic gradients thus depend on (1) the degree of concordance or discordance between two major drivers of diversity variation, namely speciation/extinction rates and resource availability, and (2) the exact form of BECA.

Although it may seem unintuitive, discordant gradients may occur in a variety of situations. For example, communities of microbes and ectothermic animals in some high latitude marine ecosystems may frequently have higher *E*/*B* compared to their tropical counterparts due to nutrient enrichment from upwelling zones elevating *E*, while colder temperature simultaneously leads to lower metabolic rates. In contrast, the tropical ecosystems may have lower $\widehat{N}$, because (1) of possible positive effects of temperature on rates of genetic divergence and speciation (Allen and Gillooly 2006; Allen et al. 2006) and (2) more stable environmental conditions due to reduced seasonality and increased climatic stability may lower rates of extinction. Therefore, in this case, the latitudinal gradient represents a complex gradient of increasing *E*/*B*, decreasing speciation, and increasing extinction with increasing latitude.

Effects of the Species Abundance Distribution

Our framework can be further developed in order to predict how the species abundance distribution and population size dependences of extinction and speciation affect mean equilibrium abundance and consequently *S* and *J* equilibria. Consider communities whose species abundance distribution at equilibrium are characterized by a probability density function $f_N(N, \widehat{N})$ with equilibrium mean species abundance $\widehat{N}$. At the beginning of a given time interval Δt, each species in a community has some abundance N that may vary among species in the community. By the end of the interval, the proportion $P_x(N)$ of species of abundance N that go extinct is a function of N. Likewise, some proportion $P_v(N)$ of the species of abundance *N* may speciate, with each speciation adding a new species to the community. $P_x(N)$ and $P_v(N)$ are equivalent to the probabilities that a species of abundance *N* goes extinct or speciates, respectively, within the time interval.

Integrating over the species abundance distribution, the community's mean total number of extinctions X_{TOT} that occur within the time interval is $S\int_0^\infty P_x(N)f_N(N,\widehat{N})dN$ and the mean total number of speciations V_{TOT} is $S\int_0^\infty P_v(N)f_N(N,\widehat{N})dN$. At equilibrium, the mean total speciation rate $(V_{TOT}/\,\Delta t)$ must be equal to the mean total extinction rate $(X_{TOT}/\,\Delta t)$, giving the equilibrium constraint formula

$$\int_0^\infty x(N)f_N(N,\widehat{N})dN = \int_0^\infty P_v(N)f_N(N,\widehat{N})dN \qquad (13)$$

By assuming functions for $P_v(N)$, $P_x(N)$, and $f_N(N)$, equation 13 can be used to solve for equilibrium mean abundance (the slope of the S-nullcline), which in conjunction with an assumed function for the J-nullcline, can be used to predict equilibrium *S* and *J* and their dependences on the parameters of extinction and speciation.

In the unrealistic, idealized scenario in which all species in the community have the same abundance ("the same-abundance distribution"), it follows from integrating Equation 13 that $\widehat{N}$ is

equal to the intersection point of $P_x(N)$ and $P_v(N)$. If instead *N* varies among species (i.e., the distribution has a positive variance), then $\widehat{N}$ can deviate from the intersection point of $P_x(N)$ and $P_v(N)$, since $f_N(N, \widehat{N})$ acts to weigh the degree to which species of different *N* contribute to the total rate of origination and extinction. For example, even if species with low *N* have low probabilities of speciation, they could be important contributors to the total rate of speciation if there are many species with low *N*. Equation 13 demonstrates that the effects of the shape of the species abundance distribution on $\widehat{N}$ are complex, depending on its interaction with $P_x(N)$ and $P_v(N)$.

Generally, with typical species abundance distributions, such as the logseries and lognormal distribution, and ecologically-relevant functions for $P_x(N)$ and $P_v(N)$, we've found that increases in the distribution's variance lead to larger values of $\widehat{N}$ (Fig. 3). This is because these distributions exhibit asymmetry with many low-abundance species and few high-abundance species. Consequently, there are many species that have higher probabilities of extinction and lower probabilities of speciation than the species with the abundance found at the intersection of $P_v(N)$ and $P_x(N)$, leading to the community as a whole needing to have a higher mean abundance in order for origination rates to balance speciation rates. Regardless, the intersection point of $P_x(N)$ and $P_v(N)$ is the main determinant of $\widehat{N}$ and shifts in $P_v(N)$ and $P_x(N)$ predictably move the S-nullcline and equilibrium *S* and *J* (Fig. 3).

Effects of speciation and extinction and their population size-dependences

In order to provide quantitative predictions of the effects of the N-dependence of speciation and extinction rates and different species-abundance distributions (SAD), we suggest the use of $\hat{J} = (\frac{E}{B})cS^{\beta}$ for the J-nullcline and derived the following baseline functions for $P_x(N)$ and $P_v(N)$ to deploy as strong starting points:

$$P_x(N) = 1 - e^{-x_0 \Delta t N^{-x_1}} \approx \Delta t x_0 N^{-x_1} \quad (14)$$

and

$$P_v(N) = 1 - e^{-v_0 \Delta t N^{v_1}} \approx \Delta t v_0 N^{v_1} \quad (15)$$

Where x_0, x_1, v_0,and v_1 are the parameters determining the rates and N-dependence of extinction and speciation, respectively, and the analytical approximations are accurate for $N \gg 1$ (Supplementary Materials). Equation 14 is derived by building on theory for extinction driven by environmental stochasticity (Ovaskainen and Meerson 2010). x_1 is mechanistically linked to population growth rate and its variance (Ovaskainen and Meerson 2010), and $x_1 \geq 0$ due to the overall negative N-dependence of extinction rate. Equations 1, 14, and 15 may be taken as operational tools to make coarse-grained predictions by quantifying the log-log slopes of the J-nullcline around equilibrium points and the slopes of $P_x(N)$ and $P_v(N)$ near their intersection points. Equation 15 thus does not discount the possibility that $P_v(N)$ is peaked nor that the J-nullcline exhibits more complex behavior (e.g., sigmoidal), as long as β around the equilibrium point varies negligibly along the gradient of interest. Alternatively, the J-nullcline and extinction functions may be taken as baseline models in their own right, as they have some theoretical and empirical support (see Supplementary Materials for derivations).

Assuming the same-abundance distribution and equations 14 and 15 approximations, ETBD predicts how equilibrium diversity, community abundance, and mean abundance should vary along gradients in the parameters governing speciation and extinction rates:

$$\hat{S} \propto (v_0/x_0)^{1/[(x_1+v_1)(1-\beta)]} \quad (16)$$

$$\hat{J} \propto (v_0/x_0)^{\beta/[(x_1+v_1)(1-\beta)]} \quad (17)$$

$$\widehat{N} \propto (x_0/v_0)^{\frac{1}{x_1+v_1}} \quad (18)$$

Importantly, equation 16 and 17 highlight that the effect of the levels of extinction (x_0) and speciation (v_0) on $\hat{S}$ and $\hat{J}$ is modulated by BECA and the degree of *N*-dependence of extinction and

396 speciation. Additionally, at equilibrium, the extinction and speciation parameters (x_1, v_1, x_0 and
397 v_0), together with BECA and *E*/*B,* determine the total rates of extinction and speciation.
398 In order to evaluate the role of the species abundance distribution in modifying the diversity
399 gradients, we determined how equilibria change along gradients in resource availability (E/B) and
400 speciation (v_0) assuming lognormal species abundance distributions with different parameters. We
401 solved equilibria numerically, as we were unable to obtain analytical solutions. The calculations
402 require solving for the value of $\widehat{N}$ that balances the total rate of extinction with the total rate of
403 speciation (Eq. 13) and then solving for the intersection of the *S* and J-nullclines (*Materials and*
404 *Methods*). Figure 4 shows that the shape of the SAD, whether the same-abundance distribution or
405 lognormal distribution with low or high variance, has minimal impact on overall changes in
406 biodiversity along gradients in speciation/extinction or resource availability, although it certainly
407 modulates equilibrium mean abundance and so it could be important to consider if the shape of the
408 SAD is suspected to change drastically over a gradient.
409
410 *Empirical Application of the Framework*
411 We applied the scaling framework to variation in tree species richness across the globe in order to
412 clarify drivers of the latitudinal diversity gradient, using a multi-scale tree biodiversity database (Keil
413 and Chase 2019)(*Materials and Methods*). Some authors argue that energy/resource availability is a
414 major driver of latitudinal diversity gradients (e.g., Wright 1983; Gaston 2000; Storch et al. 2006;
415 Hurlbert and Stegen 2014), whereas others have argued that variation in speciation or extinction
416 rate are a major driver (e.g., Fuhrman et al. 2008; Brown 2014; Rolland et al. 2014; Wu et al. 2018).
417 Since ETBD makes alternative predictions for the *S*-*J*-*E* scaling relationships depending on the role of
418 these factors, it can be used to shed light on the underpinnings of the latitudinal diversity gradient.

While ETBD deals with the scaling of diversity and abundance of communities representing large scales, high-quality abundance data for such large scales is rarely available. We therefore first checked whether a biome's average local plot-level species richness scales predictably with its regional-scale (100,000 km^2) richness, in order to determine whether ETBD's predictions have implications for across-biome variation in local richness. We found that local richness in small (0.01-0.1 km^2) and medium-sized plots (0.1-1 km^2) scales approximately linearly with regional richness (log-log slopes = 1.14 and 0.94, R^2 = 0.77 and 0.75, respectively; Fig. 5A). It's thus reasonable to use ETDB to elucidate the drivers of across-biome variation in plot-level richness. This premise accords with arguments by ecologists and biogeographers emphasizing regional and biome-scale source pools as shapers of global-scale patterns of local biodiversity (Ricklefs 1987, 2004; Cornell and Harrison 2014).

Next, we used ETBD to predict the across-biome S-J scaling relationships (Q_{SJ}) for different scenarios of diversity variation and compared predictions to the observed S-J relationships to determine which scenario manifests in trees. If across-biome diversity variation is driven entirely by resource availability (E/B), then equations 4 and 9 predict $S \propto J^1$ (i.e., $Q_{SJ} = 1$). In contrast, if diversity variation is driven entirely by a speciation/extinction gradient, then equations 5 and 9 predict $S \propto J^{1/\beta}$, where β is the scaling exponent quantifying the biodiversity effect on community abundance (BECA). Assuming $\beta = 0.26$, which is suggested by an analysis of tree diversity in forests (Liang et al. 2016*a*) and a meta-analysis of studies of BECA in primary producers (O'Connor et al. 2017), our theory predicts $S \propto J^{3.85}$ for this scenario. If instead diversity variation reflects a complex gradient involving a concordance of both drivers (i.e., $\frac{g_1}{r_1} < 0$), then equation 9 predicts the scaling exponent to be between 1 and 3.85, whereas if there is a discordance of the drivers (i.e., $\frac{g_1}{r_1} > 0$), then it predicts a scaling exponent less than 1.

For small and medium plot sizes, we found, respectively, $S \propto J^{3.72}$ and $S \propto J^{4.06}$ (R^2 = 0.69 and 0.46), where S and J are the biome-averaged species richness and total number of individuals per plot for major terrestrial biomes in the different biogeographic realms (Fig. 5B). The observed average S-J scaling is thus $S \propto J^{3.89}$, which is remarkably close to the predicted 3.85 for a purely speciation/extinction driven gradient (i.e., where $r_1 = 0$) whereas the 95% confidence intervals of the observed scaling relationships do not overlap with one as expected for a purely resource driven gradient (i.e., where $g_1 = 0$). In other words, the patterns found are in accord with the idea that tree diversity variation across biomes (and thus the latitudinal diversity gradient) is driven by the variation of speciation and extinction rates, and not resource availability.

Assuming this scenario, we can predict the rate at which species richness and community abundance should change with latitude by using use ETBD's equations. First, we estimate the value of the rate (g_1) at which the speciation/extinction balance changes with latitude from the slope of log mean abundance versus absolute latitude (equation 6), giving g_1 =0.023 (i.e., $\widehat{N} \propto 10^{0.023G}$) and $g_1 = 0.028$ (i.e., $\widehat{N} \propto 10^{0.028G}$) for small and medium-sized plots, respectively, where *G* is absolute latitude (Table 2). Using these values of g_1 we thus predict from equations 11 and 12 that $S \propto 10^{-0.031G}$ and $J \propto 10^{-0.0082G}$ in small plots and $S \propto 10^{-0.037G}$, $J \propto 10^{-0.0097G}$ in medium-sized plots. Using the mean value g_1, we also predict that at the regional-scale $S \propto 10^{-0.035G}$. These predictions are all remarkably close to and within the 95% Confidence Intervals of the observed (Fig. 5C and D, Table 2).

Discussion

We presented general quantitative theory that predicts the scaling relationships between equilibrium species richness, community abundance, and energy availability along complex environmental gradients and sheds light on the emergence of stable and unstable equilibria in

biodiversity and community abundance. ETBD shows how nullclines for richness and community abundance emerge from a few basic assumptions and are influenced by the strength of biodiversity effect on community abundance (BECA) and the multitude of geographic, genetic and ecological factors influencing extinction, speciation, and the species abundance distribution. In doing so, the theory provides a useful unifying framework for elucidating the drivers of biodiversity patterns, such as the latitudinal diversity gradient. While we used ETBD to develop general scaling theory and a baseline model involving a minimal number of assumptions, more complex scenarios of eco-evolutionary dynamics and complex gradients can be incorporated into the framework in order to address particular interactions between ecological and evolutionary processes.

Theoretical Overview

ETBD reveals shortcomings of existing biodiversity theories for explaining general patterns of diversity, including the original metabolic theory of ecology (Box 2), the MacArthur-Wilson theory of insular biogeography (MacArthur and Wilson 1967), the Neutral Theory of Biodiversity (Hubbell 2001), and their descendants (Worm & Tittensor 2018). No previous general theory of biodiversity—one that predicts biodiversity as a function of abiotic and biotic variables—has addressed the complex interactions between species richness and community abundance, namely the effect of species richness on community abundance.

Our framework unifies theories on the role of community abundance in diversity regulation due to mechanisms of "the More Individuals Hypothesis", which predicts a linear effect of community abundance on species richness (Storch et al. 2018), with work on the biodiversity-ecosystem functioning relationship (Loreau 1998; Cardinale et al. 2006; Mora et al. 2014; Liang et al. 2015; O'Connor et al. 2017; Xu et al. 2020). We found that the resulting feedbacks between biodiversity and community abundance have fundamental repercussions for the stability, scaling,

and gradients of equilibria, with the strength of the biodiversity effect on community abundance (BECA) mediating the effects of energy availability on *S* and *J*, as well as the relationship between *S* and *J* along gradients in per species extinction or speciation rates. Thus, for the purposes of macroecological predictions, community abundance cannot be taken as an independent static variable, as in prevailing biodiversity theory and models (e.g., Hubbell 2001; Brown et al. 2004; Harte 2011; but see Harte et al. 2022). Indeed, statistical analyses of geographic variation in biodiversity and community biomass/productivity, employing approaches such as structural equation models, suggest bi-causal relationships between species richness and community biomass/productivity, corroborating this point (e.g., Grace et al. 2016; Craven et al. 2020). An important finding resulting from our integration of these phenomena is that a positive BECA should lead to superlinear scaling between *S* and *J*, as well as between *S* and energy availability, in a variety of commonplace scenarios in communities experiencing competition combined with niche complementarity. This is in accord with previously enigmatic observations of superlinear scaling (Brown 2014; Storch et al. 2018; Hamilton et al. 2020). Importantly, ETBD shows that all persistent communities (communities that aren't on a path to extinction) have at least one stable equilibrium in biodiversity and community abundance. This stable equilibrium emerges from two universal constraints to biodiversity dynamics—that (1) the curves quantifying the population size–dependence of extinction and origination must necessarily intersect and (2) BECA is ultimately constrained by thermodynamic limits to community abundance. Even when communities aren't at equilibrium, these attractors can shape biodiversity patterns in two ways. First, many communities appear to hover around equilibrium points, as suggested by accumulating evidence from macroecological and macroevolutionary analyses (Rabosky 2009, 2022; Rabosky and Hurlbert 2015; Storch and Okie 2019; Rineau et al. 2022; Šímová et al. 2023), which would lead to their average species richness being close to their equilibrium points. Secondly, following a major global-scale

perturbation that pushes communities out of equilibrium, all-else-being-equal, the non-equilibrium communities with higher stable equilibria are more likely to have greater species richness than the non-equilibrium communities with lower stable equilibria, both because these communities have a greater "distance" to fall from and because the further a community is from a stable equilibrium point, the greater its rate of increase in diversity, leading to the high-equilibria community bouncing back to a higher richness more quickly. While these points may seem trivial, they can help resolve longstanding debates regarding the role of "cradles", "museums", and "graves" in shaping global-scale biodiversity patterns (Vasconcelos et al. 2022).

The Latitudinal Diversity Gradient in Trees

Application of our framework to global-scale variation in tree biodiversity suggests that tree diversity variation is driven by variation in the speciation and extinction probabilities whose effects are modulated by the biodiversity-ecosystem functioning relationship, whereas energy availability (E/B, i.e., maximum attainable community abundance) plays a negligible role. We suspect three non-mutually exclusive explanations for the surprising finding of this apparent negligible role of energy/resource availability. First, maximum attainable community abundance (per unit area) may be strongly limited by space (e.g., as implied by Enquist et al. 2009; West et al. 2009), which would not vary across biomes, and the size of trees, which does not vary strongly with latitude (Stegen et al. 2011). Second, any variation in maximum energy supply (E) across biomes may be balanced by co-variation in individual metabolic rate (B), with trees having higher metabolic rates in higher energy environments, such that maximum attainable community abundance (E/B) varies little across biomes. The prediction and observation that forest stand biomass is invariant of mean annual temperature and latitude corroborates this point (Enquist and Niklas 2001; Stegen et al. 2011). Third, per species speciation and/or extinction rates vary substantially across biomes, due to

differences in seasonality, climatic fluctuations from Glacial-Interglacial Cycles, possible temperature-driven differences in rates of genetic divergence, and other factors.

Our finding may seem to contrast with work emphasizing the role of ecosystem productivity (such as NPP) in generating macroscale biodiversity patterns (e.g., Bohdalková et al. 2021), but it does not exclude a role for total energy or resource supply (*E*) in biodiversity regulation. Energy availability (in terms of the resource inflow) may play a more important role in biodiversity patterns of consumers, especially endotherms whose individual metabolic rates co-vary little with ecosystem production. More importantly, energy availability, according to ETBD, always plays a crucial role in stabilizing diversity dynamics even when it does not directly drive spatial diversity variation.

The Biodiversity Effect on Community Abundance (BECA)

In our analysis of tree diversity, the scaling of *S* with *J* was remarkably well-predicted assuming the exponent β for the BECA of 0.26. This support for ETBD predictions with $0 < \beta < 1$ suggests these biomes hover around their upper tree diversity equilibrium points at which partially-overlapping niches and competition mediate the BECA, as opposed to a possible lower stable equilibrium point created by $\beta > 1$ where the effects of interspecific facilitation would dominate. Since β is far from zero, many communities with relatively lower species richness are far from their absolute maximum community abundances imposed by thermodynamic limits. This corroborates analyses of a variety of manipulative biodiversity experiments underscoring the pervasiveness of a positive BECA (Tilman et al. 2001; Bell et al. 2005; e.g., Cardinale et al. 2006; O'Connor et al. 2017; Qiu and Cardinale 2020), with the majority of exponents quantifying the effects of species richness on community biomass, productivity, and resource availability being between 0 and 1, averaging 0.26, (O'Connor et al. 2017) and reported to be 0.26 for the effect of richness on tree community productivity in forests (Liang et al. 2016*b*).

In plants, the positive BECA can be expected, among other things, to result from the differing effects of species in modulating biomass loss due to herbivory and diseases, the role that different species play in re-shaping nutrient limitations to growth, and other factors related to niche efficiency and complementarity (e.g., Loreau 1998; Liang et al. 2015; Wright et al. 2017). In consumer communities, different species can vary substantially in their ability to acquire and metabolize different resources. Many resources go unused by animals, contributing instead to decomposer pools, and the introduction of an animal with an innovation in foraging or digestion can improve the acquisition or assimilation of a resource (e.g., DeMiguel et al. 2014; Pyenson 2017), increasing the fraction of total energy that is converted into community abundances.

Our theory and analyses underscore a need to better understand the fundamental quantitative features of BECA. Although the scaling exponent of the J-nullcline could depend on spatial scale (Gonzalez et al. 2020; Barry et al. 2021), the actual extent of this scale-dependence is unknown and a positive effect of diversity is expected to hold across scales (Gonzalez et al. 2020; Qiu and Cardinale 2020). Throughout Earth history, biological diversification has repeatedly expanded the total energy budget and biomass of biomes and the biosphere (Kennedy et al. 2006; David and Alm 2011; Erwin et al. 2011), indicating the effects of biodiversity on community abundance at scales of biomes and the Earth system. Determining the strength of this biodiversity effect at these large scales is an important but challenging avenue for future research. Addressing the severe gaps in contemporary and paleontological abundance data, particularly for entire communities or assemblages (Dirzo et al. 2014), is crucial for this endeavor and for using ETBD to evaluate the role of community abundance and resource availability in shaping patterns and trajectories of biodiversity.

584 *Emergence of multiple biodiversity equilibria*

585 While the role of interspecific interactions in creating multiple equilibria in community structure or
586 ecosystem properties has been previously recognized (e.g., Holling 1973; Sutherland 1974; Scheffer
587 et al. 2001; Konar and Estes 2003), we have outlined a general theory that quantifies the effects of
588 niches, competition, and facilitation, as well as nonlinearities in the population size-dependence of
589 extinction and speciation, in creating multiple equilibria in biodiversity and community abundance
590 (Box 1). As such, ETBD provides a formal quantitative framework for informing qualitative
591 arguments over the existence of planetary-scale tipping points (e.g., Brook et al. 2013; Lenton and
592 Williams 2013) and the role of facilitation and ecosystem engineering in shaping historical patterns
593 of diversification and biosphere modification (Jones et al. 1994). Our theory demonstrates how
594 planetary scale tipping points could emerge more readily than previously thought (Brook et al.
595 2013). In any case, just as many ecosystems appear to have multiple stable states in key ecosystem
596 properties (Scheffer et al. 2001; Kéfi et al. 2016), ETBD suggests that many local and biome-scale
597 ecological systems could have multiple stable biodiversity equilibria. Consideration of such multiple
598 stable equilibria and critical thresholds that emerge from facilitation may be vital towards
599 understanding some historical and geographic shifts in biodiversity and biomass, as well as
600 biodiversity responses to human-induced changes in the Anthropocene (Storch et al. 2022).
601
602 *Concluding Remarks*
603 We have presented a theory that integrates major processes underlying diversity dynamics into a
604 single predictive framework. A strength of the framework is that it combines generality with
605 flexibility. The theory concerning the scaling of *S* and *J* along environmental gradients makes
606 baseline predictions that do not require making specific assumptions about ecological or
607 evolutionary mechanisms, while specific mathematical models can also be implemented to address

608 particular scenarios of evolution, community assembly, or global change. For example, under
609 neutral community assembly, the species abundance distribution is a logseries distribution, whereas
610 under purely niche-based assembly, the species abundance distribution tends towards a lognormal
611 distribution (Pueyo et al. 2007). ETBD can accommodate either extreme of assembly, as well as the
612 neutral-niche continuum, by assuming one of these species abundance distributions or a
613 generalized species abundance distribution quantifying the entire assembly continuum (Pueyo et al.
614 2007). The theory can also be used to evaluate specific scenarios in which assembly, ecosystem
615 functioning, speciation, or extinction are hypothesized to change along an environmental gradient
616 or with global change (e.g., Box 2), pointing to future directions for developing a predictive ecology
617 of biodiversity change in the Anthropocene. While ETBD is not a substitute for processed-based
618 simulation models of biodiversity dynamics (Rangel et al. 2018; Pontarp et al. 2019), it
619 demonstrates the continued usefulness of mathematical theory in macroecology and points to
620 crucial eco-evolutionary phenomena that should be addressed in detailed biodiversity models.
621

622 **Materials and Methods**

623 *Solving for Equilibrium S and J*

624 In order to predict how *S* and *J* should change as a function of parameters of extinction, speciation,
625 and the species abundance distribution, specific functions need to be assumed or derived for $P_x(N)$,
626 $P_v(N)$, and the species abundance distribution. Assuming a lognormal species abundance
627 distribution and the functions we derived for extinction and speciation (Eq. 14 & 15, Supporting
628 Online Material), the integration of the equilibrium constraint formula(Equation 13) cannot be
629 solved analytically. We used MATLAB 2021a (Mathworks 2021) and its function *integral* to
630 numerically solve the integrals for equilibrium mean abundance $\widehat{N}$–that is, for the slope of the S-
631 nullcline. $\hat{S}$ and $\hat{J}$ were then calculated algebraically by solving for the intersection of the S and J-

nullclines–that is, $\hat{S} = [c\widehat{N}^{-1}(E/B)]^{1/(1-\beta)}$ and $\hat{J} = [c\widehat{N}^{-\beta}(E/B)]^{1/(1-\beta)}$. As the lognormal distribution is a two-parameter distribution (σ and μ), a value for one of its parameters must be assumed in order to solve for the other parameter and thus $\widehat{N}$ (since in a lognormal distribution $\widehat{N} = e^{\mu+\sigma^2/2}$). As μ represents the mean of log *N* whereas σ represents the standard deviation of log *N,* the baseline theoretical expectation is to attribute variation in $\widehat{N}$ along a gradient to variation in μ and so assume that σ does not change along the gradients. Equation 13 is used to solve for μ and then $\widehat{N}$ can be calculated from the relation between mean and μ in the lognormal distribution (i.e., from $\widehat{N} = e^{\mu+\sigma^2/2}$).

Data & Analysis

We used a global tree species richness database produced by Keil et al. (Keil and Chase 2019). The data include the species richness and total number of individual stems counted in plots of different sizes ranging from 0.0001 km^2 to 0.5 km^2, estimates of tree species richness and total number of individual trees for countries of the world and the States of the USA, and estimates of mean annual air temperature of plots and countries. Additionally, Keil and Chase (2019) categorized the biome and biogeographic realm that each plot and country is located in.

Before analyzing the data within the ETDB framework, we further curated and standardized the data in the following ways in order to increase its appropriateness for our macroecological analysis. To remove the confounding effects of isolation on biodiversity, we removed all plots and countries located on islands from our analysis. A few plots were in environments highly disturbed by humans (e.g., clear-cut forests) and so they also have been removed. The minimum diameter at base height (DBH) of trees varied some between studies, but the majority had minimum DBHs of 10 cm. To mitigate the contribution of the variation in DBH as a confounding factor, we only included plots with a minimum DBH of 10 cm.

Country/state-level data. We used the country/state level data to estimate the average regional-scale species richness of each biome-realm combination available in the database (e.g., "Tropical and Subtropical Moist Broadleaf Forests - Indo-Malay" and "Tropical and Subtropical Moist Broadleaf Forests - Afrotropic"). Specifically, we estimated the average number of species per 100,000 km^2 for each biome-realm combination in the following way. For each biome-realm combination, we performed an ordinary least-squares regression analysis of the log of country/state species richness versus the log of country/state area for all the countries/states found in that biome-realm combination. We then used the parameterized regression model for each biome-realm combination to estimate the number of species per 100,000 km^2 for each country in that biome-realm combination (i.e., regional species richness). This approach normalizes for variation in the areas of countries, thereby removing area as a confounding variable. For each biome-realm combination, we then calculated the mean of log regional species richness (Table S3).

Plot-level data. We binned the plot data according to plot area, using bin widths of one order of magnitude. In practice most of the bins had much lower variation in plot sizes, as the bins were mostly made up of plots of similar standard areas (and minimum DBH). The bin for plots of 0.01 to less than 0.1 km^2 was almost entirely made up of plots of 0.01 km^2, so we only included plots of 0.01 km^2 for this bin, in order to reduce confounding error. The bin for plots of 0.1 to less than 1 km^2 had plot areas varying from 0.14 km^2 to 0.5 km^2 with the majority having sizes of 0.2-0.25 km^2. For each plot area bin, we calculated the mean of the following variables for each biome-realm combination: log species richness, log number of individuals, mean annual air temperature, and mean absolute latitude (Table S3).

Diversity gradient analysis. We used Reduced Major Axis regression to determine the relationships between variables, log-transforming variables when appropriate in order to linearize the expected relationship between variables. We used MATLAB R2021a and the formulas from

Niklas (Niklas 1994) to calculate parameter values and their 95% Confidence Intervals. Reduced Major Axis regression was chosen because it is a Type II regression model (Sokal and Rohlf 1981) employed for estimating the parameter values of functional, structural, scaling, or law-like relationships between variables (McArdle 1988; Smith 2009). To evaluate the sensitivity of our results to our method for calculating regional species richness, we also repeated all regional species richness analyses (local versus regional richness and regional richness versus absolute latitude) using raw country/state richness data without implementing the normalization for variation in country/state area. In other words, for each biome-realm combination, we calculated the mean log country/state species richness and repeated the previously described local-regional scaling and gradient analyses on this measure of regional richness. The results from this analysis were similar to our other findings (Table S1).

References

Allen, A. P., J. H. Brown, and J. F. Gillooly. 2002. Global biodiversity, biochemical kinetics, and the energetic-equivalence rule. Science 297:1545–1548.

Allen, A. P., and J. F. Gillooly. 2006. Assessing latitudinal gradients in speciation rates and biodiversity at the global scale. Ecology Letters 9:947–954.

Allen, A. P., J. F. Gillooly, V. M. Savage, and J. H. Brown. 2006. Kinetic effects of temperature on rates of genetic divergence and speciation. Proceedings of the National Academy of Sciences 103:9130–9135.

Allen, A. P., and V. M. Savage. 2007. Setting the absolute tempo of biodiversity dynamics. Ecology letters 10:637–646.

Barry, K. E., G. A. Pinter, J. W. Strini, K. Yang, I. G. Lauko, S. A. Schnitzer, A. T. Clark, et al. 2021. A graphical null model for scaling biodiversity–ecosystem functioning relationships. Journal of Ecology 109:1549–1560.

Bell, T., J. A. Newman, B. W. Silverman, S. L. Turner, and A. K. Lilley. 2005. The contribution of species richness and composition to bacterial services. Nature 436:1157–1160.

Bohdalková, E., A. Toszogyova, I. Šímová, and D. Storch. 2021. Universality in biodiversity patterns: variation in species–temperature and species–productivity relationships reveals a prominent role of productivity in diversity gradients. Ecography 44:1366–1378.

Brook, B. W., E. C. Ellis, M. P. Perring, A. W. Mackay, and L. Blomqvist. 2013. Does the terrestrial biosphere have planetary tipping points? Trends in ecology & evolution 28:396–401.

Brown, J. H. 2014. Why are there so many species in the tropics? Journal of biogeography 41:8–22.

Brown, J. H., J. F. Gillooly, A. P. Allen, V. M. Savage, and G. B. West. 2004. Toward a metabolic theory of ecology. Ecology 85:1771–1789.

Cardinale, B. J., M. A. Palmer, and S. L. Collins. 2002. Species diversity enhances ecosystem functioning through interspecific facilitation. Nature 415:426–429.

Cardinale, B. J., D. S. Srivastava, J. E. Duffy, J. P. Wright, A. L. Downing, M. Sankaran, and C. Jouseau. 2006. Effects of biodiversity on the functioning of trophic groups and ecosystems. Nature 443:989–992.

717 Castillo, J. M., B. Gallego-Tévar, E. M. Castellanos, M. E. Figueroa, and A. J. Davy. 2021. Primary succession in
718 an Atlantic salt marsh: From intertidal flats to mid-marsh platform in 35 years. Journal of Ecology 109:2909–
719 2921.
720 Connell, J. H., and R. O. Slatyer. 1977. Mechanisms of succession in natural communities and their role in
721 community stability and organization. The american naturalist 111:1119–1144.
722 Cornell, H. V., and S. P. Harrison. 2014. What are species pools and when are they important? Annual Review
723 of Ecology, Evolution, and Systematics 45:45–67.
724 Craven, D., M. T. Van Der Sande, C. Meyer, K. Gerstner, J. M. Bennett, D. P. Giling, J. Hines, et al. 2020. A
725 cross-scale assessment of productivity–diversity relationships. (M. Mayfield, ed.)Global Ecology and
726 Biogeography 29:1940–1955.
727 Currie, D. J., G. G. Mittelbach, H. V. Cornell, R. Field, J. F. Guegan, B. A. Hawkins, D. M. Kaufman, et al. 2004.
728 Predictions and tests of climate-based hypotheses of broad-scale variation in taxonomic richness. Ecology
729 Letters 7:1121–1134.
730 David, L. A., and E. J. Alm. 2011. Rapid evolutionary innovation during an Archaean genetic expansion. Nature
731 469:93–96.
732 DeMiguel, D., B. Azanza, and J. Morales. 2014. Key innovations in ruminant evolution: a paleontological
733 perspective. Integrative zoology 9:412–433.
734 Dirzo, R., H. S. Young, M. Galetti, G. Ceballos, N. J. B. Isaac, and B. Collen. 2014. Defaunation in the
735 Anthropocene. Science 345:401–406.
736 Enquist, B. J., and K. J. Niklas. 2001. Invariant scaling relations across tree-dominated communities. Nature
737 410:655–660.
738 Enquist, B. J., G. B. West, and J. H. Brown. 2009. Extensions and evaluations of a general quantitative theory
739 of forest structure and dynamics. Proceedings of the National Academy of Sciences 106:7046.
740 Erwin, D. H., M. Laflamme, S. M. Tweedt, E. A. Sperling, D. Pisani, and K. J. Peterson. 2011. The Cambrian
741 conundrum: early divergence and later ecological success in the early history of animals. science 334:1091–
742 1097.
743 Etienne, R. S., J. S. Cabral, O. Hagen, F. Hartig, A. H. Hurlbert, L. Pellissier, M. Pontarp, et al. 2019. A minimal
744 model for the latitudinal diversity gradient suggests a dominant role for ecological limits. The American
745 Naturalist 194:E122–E133.
746 Field, R., B. A. Hawkins, H. V. Cornell, D. J. Currie, J. A. F. Diniz-Filho, J. Guégan, D. M. Kaufman, et al. 2009.
747 Spatial species-richness gradients across scales: a meta-analysis. Journal of Biogeography 36:132–147.
748 Fine, P. V. 2015. Ecological and evolutionary drivers of geographic variation in species diversity. Annual
749 Review of Ecology, Evolution, and Systematics 46:369–392.
750 Fuhrman, J. A., J. A. Steele, I. Hewson, M. S. Schwalbach, M. V. Brown, J. L. Green, and J. H. Brown. 2008. A
751 latitudinal diversity gradient in planktonic marine bacteria. Proceedings of the National Academy of Sciences
752 105:7774–7778.
753 Gaston, K. J. 2000. Global patterns in biodiversity. Nature 405:220–227.
754 Gavrilets, S. 2003. Perspective: models of speciation: what have we learned in 40 years? Evolution 57:2197–
755 2215.
756 Gonzalez, A., R. M. Germain, D. S. Srivastava, E. Filotas, L. E. Dee, D. Gravel, P. L. Thompson, et al. 2020.
757 Scaling-up biodiversity-ecosystem functioning research. Ecology Letters 23:757–776.
758 Grace, J. B., T. M. Anderson, E. W. Seabloom, E. T. Borer, P. B. Adler, W. S. Harpole, Y. Hautier, et al. 2016.
759 Integrative modelling reveals mechanisms linking productivity and plant species richness. Nature 529:390–
760 393.
761 Griffen, B. D., and J. M. Drake. 2008. A review of extinction in experimental populations. Journal of Animal
762 Ecology 77:1274–1287.
763 Hamilton, M. J., R. S. Walker, and C. P. Kempes. 2020. Diversity begets diversity in mammal species and
764 human cultures. Scientific reports 10:1–11.
765 Harte, J. 2011. Maximum entropy and ecology: a theory of abundance, distribution, and energetics. Oxford
766 University Press.
767 Harte, J., M. Brush, E. A. Newman, and K. Umemura. 2022. An equation of state unifies diversity,
768 productivity, abundance and biomass. Communications Biology 5:1–6.

769 Hawkins, B. A., C. M. McCain, T. J. Davies, L. B. Buckley, B. L. Anacker, H. V. Cornell, E. I. Damschen, et al.
770 2012. Different evolutionary histories underlie congruent species richness gradients of birds and mammals.
771 Journal of Biogeography 39:825–841.
772 Holling, C. S. 1973. Resilience and stability of ecological systems. Annual review of ecology and systematics
773 4:1–23.
774 Hubbell, S. P. 2001. The unified neutral theory of biodiversity and biogeography Princeton University Press.
775 Princeton, New Jersey, USA.
776 Hurlbert, A. H., and J. C. Stegen. 2014. When should species richness be energy limited, and how would we
777 know? Ecology letters 17:401–413.
778 Jones, C. G., J. H. Lawton, and M. Shachak. 1994. Organisms as ecosystem engineers. Oikos 373–386.
779 ———. 1997. Positive and negative effects of organisms as physical ecosystem engineers. Ecology 78:1946–
780 1957.
781 Kéfi, S., M. Holmgren, and M. Scheffer. 2016. When can positive interactions cause alternative stable states
782 in ecosystems? Functional Ecology 30:88–97.
783 Keil, P., and J. M. Chase. 2019. Global patterns and drivers of tree diversity integrated across a continuum of
784 spatial grains. Nature ecology & evolution 3:390–399.
785 Kennedy, M., M. Droser, D. Pevear, and D. Mrofka. 2006. Late Precambrian oxygenation; inception of the clay
786 mineral factory. Science 311:1446–1449.
787 Kjær, U., S. L. Olsen, and K. Klanderud. 2018. Shift from facilitative to neutral interactions by the cushion
788 plant Silene acaulis along a primary succession gradient. Journal of Vegetation Science 29:42–51.
789 Konar, B., and J. A. Estes. 2003. The stability of boundary regions between kelp beds and deforested areas.
790 Ecology 84:174–185.
791 Lenton, T. M., and H. T. Williams. 2013. On the origin of planetary-scale tipping points. Trends in Ecology &
792 Evolution 28:380–382.
793 Liang, J., T. W. Crowther, N. Picard, S. Wiser, M. Zhou, G. Alberti, E.-D. Schulze, et al. 2016*a*. Positive
794 biodiversity-productivity relationship predominant in global forests. Science 354.
795 ———. 2016*b*. Positive biodiversity-productivity relationship predominant in global forests. Science 354.
796 Liang, J., M. Zhou, P. C. Tobin, A. D. McGuire, and P. B. Reich. 2015. Biodiversity influences plant productivity
797 through niche–efficiency. Proceedings of the national academy of sciences 112:5738–5743.
798 Loreau, M. 1998. Biodiversity and ecosystem functioning: a mechanistic model. Proceedings of the National
799 Academy of Sciences 95:5632–5636.
800 MacArthur, R. H., and E. O. Wilson. 1967. The theory of island biogeography. Princeton University Press,
801 Princeton, New Jersey.
802 Mathworks, M. 2021. MATLAB 2021a. The MathWorks: Natick, MA, USA.
803 McArdle, B. H. 1988. The structural relationship: regression in biology. Canadian Journal of Zoology 66:2329–
804 2339.
805 McDonald, K. A., and J. H. Brown. 1992. Using montane mammals to model extinctions due to global change.
806 Conservation Biology 6:409–415.
807 McGill, B. J. 2019. The what, how and why of doing macroecology. Global Ecology and Biogeography 28:6–17.
808 Mora, C., R. Danovaro, and M. Loreau. 2014. Alternative hypotheses to explain why biodiversity-ecosystem
809 functioning relationships are concave-up in some natural ecosystems but concave-down in manipulative
810 experiments. Scientific Reports 4:1–9.
811 Morris, B. E., R. Henneberger, H. Huber, and C. Moissl-Eichinger. 2013. Microbial syntrophy: interaction for
812 the common good. FEMS microbiology reviews 37:384–406.
813 Nijs, I., and J. Roy. 2000. How important are species richness, species evenness and interspecific differences
814 to productivity? A mathematical model. Oikos 88:57–66.
815 Niklas, K. J. 1994. Plant allometry: the scaling of form and process. Univ. Chicago Press.
816 O'Connor, M. I., A. Gonzalez, J. E. Byrnes, B. J. Cardinale, J. E. Duffy, L. Gamfeldt, J. N. Griffin, et al. 2017. A
817 general biodiversity–function relationship is mediated by trophic level. Oikos 126:18–31.
818 Okie, J. G., and J. H. Brown. 2009. Niches, body sizes, and the disassembly of mammal communities on the
819 Sunda Shelf islands. Proc. Natl. Acad. Sci. U.S.A. 106:19679–19684.
820 Ovaskainen, O., and B. Meerson. 2010. Stochastic models of population extinction. Trends in ecology &
821 evolution 25:643–652.

Pimm, S. L., H. L. Jones, and J. Diamond. 1988. On the risk of extinction. The American Naturalist 132:757–785.

Pontarp, M., L. Bunnefeld, J. S. Cabral, R. S. Etienne, S. A. Fritz, R. Gillespie, C. H. Graham, et al. 2019. The latitudinal diversity gradient: novel understanding through mechanistic eco-evolutionary models. Trends in ecology & evolution 34:211–223.

Pueyo, S., F. He, and T. Zillio. 2007. The maximum entropy formalism and the idiosyncratic theory of biodiversity. Ecology Letters 10:1017–1028.

Pyenson, N. D. 2017. The ecological rise of whales chronicled by the fossil record. Current Biology 27:R558–R564.

Qiu, J., and B. J. Cardinale. 2020. Scaling up biodiversity–ecosystem function relationships across space and over time. Ecology 101:e03166.

Rabosky, D. L. 2009. Ecological limits and diversification rate: alternative paradigms to explain the variation in species richness among clades and regions. Ecology letters 12:735–743.

———. 2022. Evolutionary time and species diversity in aquatic ecosystems worldwide. Biological Reviews.

Rabosky, D. L., and A. H. Hurlbert. 2015. Species richness at continental scales is dominated by ecological limits. The American Naturalist 185:572–583.

Rangel, T. F., N. R. Edwards, P. B. Holden, J. A. F. Diniz-Filho, W. D. Gosling, M. T. P. Coelho, F. A. Cassemiro, et al. 2018. Modeling the ecology and evolution of biodiversity: Biogeographical cradles, museums, and graves. Science 361:eaar5452.

Reich, P. B., D. Tilman, F. Isbell, K. Mueller, S. E. Hobbie, D. F. Flynn, and N. Eisenhauer. 2012. Impacts of biodiversity loss escalate through time as redundancy fades. Science 336:589–592.

Ricklefs, R. E. 1987. Community diversity: relative roles of local and regional processes. Science 235:167–171.

———. 2004. A comprehensive framework for global patterns in biodiversity. Ecology letters 7:1–15.

Rineau, V., J. Smyčka, and D. Storch. 2022. Diversity dependence is a ubiquitous phenomenon across Phanerozoic oceans. Science Advances 8:eadd9620.

Rolland, J., F. L. Condamine, F. Jiguet, and H. Morlon. 2014. Faster speciation and reduced extinction in the tropics contribute to the mammalian latitudinal diversity gradient. PLoS biology 12:e1001775.

Rosenzweig, M. L. 1995. Species diversity in space and time. Cambridge Univ Pr.

Scheffer, M., S. Carpenter, J. A. Foley, C. Folke, and B. Walker. 2001. Catastrophic shifts in ecosystems. Nature 413:591–596.

Šímová, I., A. Ordonez, and D. Storch. 2023. The dynamics of the diversity–energy relationship during the last 21,000 years. Global Ecology and Biogeography 32:707–718.

Smith, R. J. 2009. Use and misuse of the reduced major axis for line-fitting. American journal of physical anthropology 140:476–486.

Sokal, R. R., and F. J. Rohlf. 1981. Biometry: the principles and practice of statistics in biological research. WH Freeman New York.

Stegen, J. C., N. G. Swenson, B. J. Enquist, E. P. White, O. L. Phillips, P. M. Jørgensen, M. D. Weiser, et al. 2011. Variation in above-ground forest biomass across broad climatic gradients. Global Ecology and Biogeography 20:744–754.

Storch, D. 2012. Biodiversity and its energetic and thermal controls. Metabolic ecology: a scaling approach 120–131.

Storch, D., E. Bohdalková, and J. Okie. 2018. The more-individuals hypothesis revisited: the role of community abundance in species richness regulation and the productivity–diversity relationship. Ecology letters 21:920–937.

Storch, D., R. G. Davies, S. Zajíček, C. D. L. Orme, V. Olson, G. H. Thomas, T.-S. Ding, et al. 2006. Energy, range dynamics and global species richness patterns: reconciling mid-domain effects and environmental determinants of avian diversity. Ecology Letters 9:1308–1320.

Storch, D., and J. G. Okie. 2019. The carrying capacity for species richness. Global Ecology and Biogeography 28:1519–1532.

Storch, D., I. Šímová, J. Smyčka, E. Bohdalková, A. Toszogyova, and J. G. Okie. 2022. Biodiversity dynamics in the Anthropocene: how human activities change equilibria of species richness. Ecography 2022.

Sutherland, J. P. 1974. Multiple stable points in natural communities. The American Naturalist 108:859–873.

874 Tilman, D., P. B. Reich, J. Knops, D. Wedin, T. Mielke, and C. Lehman. 2001. Diversity and productivity in a
875 long-term grassland experiment. Science 294:843–845.
876 Vasconcelos, T., B. C. O'Meara, and J. M. Beaulieu. 2022. Retiring "cradles" and "museums" of biodiversity.
877 The American Naturalist 199:194–205.
878 Walker, L. R., and R. Del Moral. 2003. Primary succession and ecosystem rehabilitation. Cambridge University
879 Press.
880 West, G. B., B. J. Enquist, and J. H. Brown. 2009. A general quantitative theory of forest structure and
881 dynamics. Proceedings of the National Academy of Sciences 106:7040.
882 Worm, B., and D. P. Tittensor. 2018. A theory of global biodiversity. A Theory of Global Biodiversity. Princeton
883 University Press.
884 Wright, A. J., D. A. Wardle, R. Callaway, and A. Gaxiola. 2017. The overlooked role of facilitation in
885 biodiversity experiments. Trends in Ecology & Evolution 32:383–390.
886 Wright, D. H. 1983. Species-energy theory: an extension of species-area theory. Oikos 41:496–506.
887 Wu, B., F. Liu, M. D. Weiser, D. Ning, J. G. Okie, L. Shen, J. Li, et al. 2018. Temperature determines the
888 diversity and structure of N2O-reducing microbial assemblages. Functional ecology 32:1867–1878.
889 Xu, S., N. Eisenhauer, O. Ferlian, J. Zhang, G. Zhou, X. Lu, C. Liu, et al. 2020. Species richness promotes
890 ecosystem carbon storage: evidence from biodiversity-ecosystem functioning experiments. Proceedings of
891 the Royal Society B 287:20202063.
892

893

894 **Acknowledgements**

895 We thank Drew Allen, Fangliang He, Levi Gray, Robert Pacák, Honza Smyčka, Anna Toszogyova, the
896 Storch research group, and the Network for Ecological Theory Integration (NETI) for helpful
897 discussions and support, and Dan Rabosky, Allen Hurlbert, and an anonymous reviewer for valuable
898 feedback on the manuscript.

899

900 **Funding:** The project was supported by the Czech Science Foundation (grant number 20-29554X), by
901 the National Aeronautics and Space Administration (NNX16AJ61G, to JGO), and an International
902 Mobility Fellowship from Charles University (to JGO).

903

904 **Author contributions:** JGO and DS conceived the theory; JO developed the mathematical
905 framework and models; JGO and DS contributed to visualization; JO analyzed the data; DS provided
906 feedback on theory development and analysis; JO wrote the first draft; JO and DS revised the draft.

907

908 **Competing Interests:** Authors declare that they have no competing interests.

909

910 **Data and materials availability:** All data are available at Keil and Chase (Keil and Chase 2019).

911

Figures, Tables, and Boxes

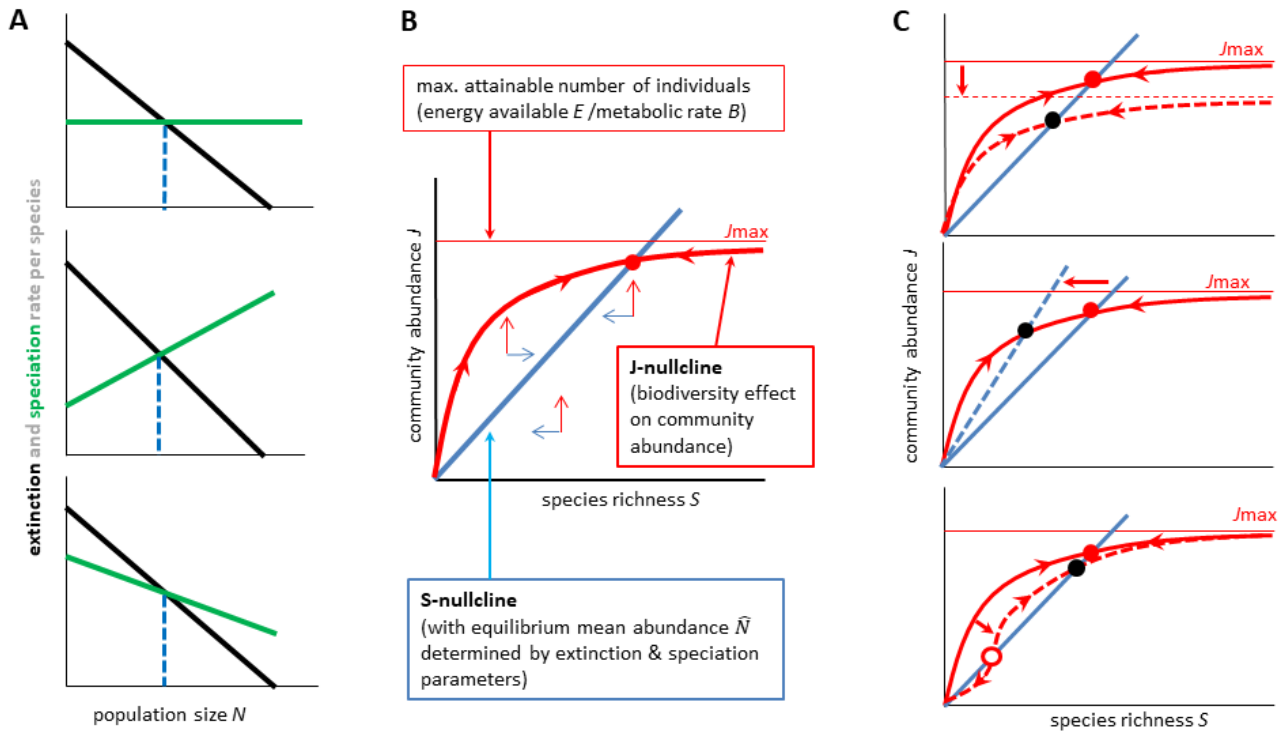

Figure 1. The foundations of the Equilibrium Theory of Biodiversity Dynamics (ETBD). (**A**) Origination (green) and extinction (black) rates depend on population size in various ways, but around their intersection point the extinction curve has a more negative slope than the origination rate. This intersection indicates the existence of a population size at which origination and extinction rates are equal. (**B**) In the phase plane for species richness *S* and community abundance *J*, this implies a diagonal line (S-nullcline, blue line) with a slope determined by equilibrium mean population size $\widehat{N}$, which depends on the intersection of the lines in panel A and the species abundance distribution. This *S*-nullcline indicates values of *S* and *J* in which total speciation rate is equal to total extinction rate. Points directly to the right of this line represent communities where $J/S < \widehat{N}$; mean population size is thus smaller than $\widehat{N}$, leading to extinction rate being higher than speciation rate and the system having the tendency to move back towards the S-nullcline. The opposite happens if $J/S > \widehat{N}$ (left from the *S*-nullcline). Equilibrium *S* and *J* occur at the intersection

(solid red point) of the S-nullcline with the *J*-nullcline (thick red line), which quantifies the effects of biodiversity on community abundance (BECA). The J-nullcline may take a variety of forms, but eventually plateaus, being constrained by energy availability (thin red line). Perturbed communities below the J-nullcline follow upward trajectories converging on the J-nullcline, whereas out-of-equilibrium communities above the J-nullcline follow downward converging trajectories. Once on the J-nullcline, trajectories flow along the J-nullcline in the direction determined by their position with respect to the S-nullcline. (**C**) The position of equilibria can change with changing (1) energy availability (top), (2) origination and/or extinction rates that affect mean equilibrium abundance and thus the S-nullcline (middle), or (3) the shape of the J-nullcline (bottom). If the J-nullcline has a more complex shape, there can be multiple equilibria, both stable and unstable (empty circle). Unstable equilibria on this S-nullcline emerge when this S-nullcline is crossed by a J-nullcline with a steeper slope than the S-nullcline.

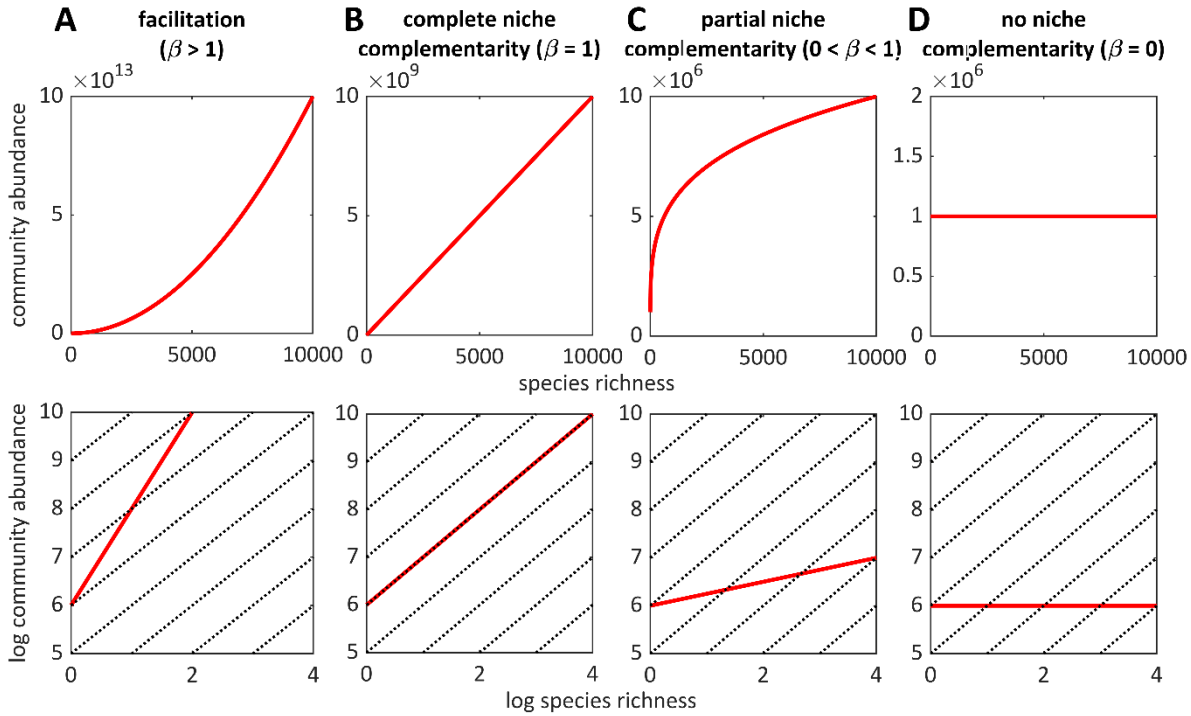

Figure 2. Interspecific facilitation, niche complementarity, and competition shape the community abundance nullcline (J-nullcline), which reflects the effect of biodiversity on equilibrium community

abundance (BECA). The scaling exponent β is the slope of the J-nullcline in log-log space (bottom row of panels) and quantifies the strength of the BECA. Red lines illustrate different hypothetical J-nullclines and dashed lines with $\beta = 1$ are shown for comparison. (**A**) When facilitation pervades, adding species to a community leads to a disproportionate increase in community abundance. (**B**) If there is no facilitation but each species in the community has a unique niche (e.g., does not compete with other species for resources), then adding species to a community leads to a linear increase in community abundance. (**C**) If species have niches that are partially complementary and partially overlapping due to competing for shared resources, then adding species to a community leads to a less than proportional increase in community abundance. (**D**) If, instead, all species have identical niches, then species richness has no effect on community abundance. Note that in all scenarios, the J-nullcline plateaus at some maximum (not shown here), at which point β approaches zero, as in **D.**

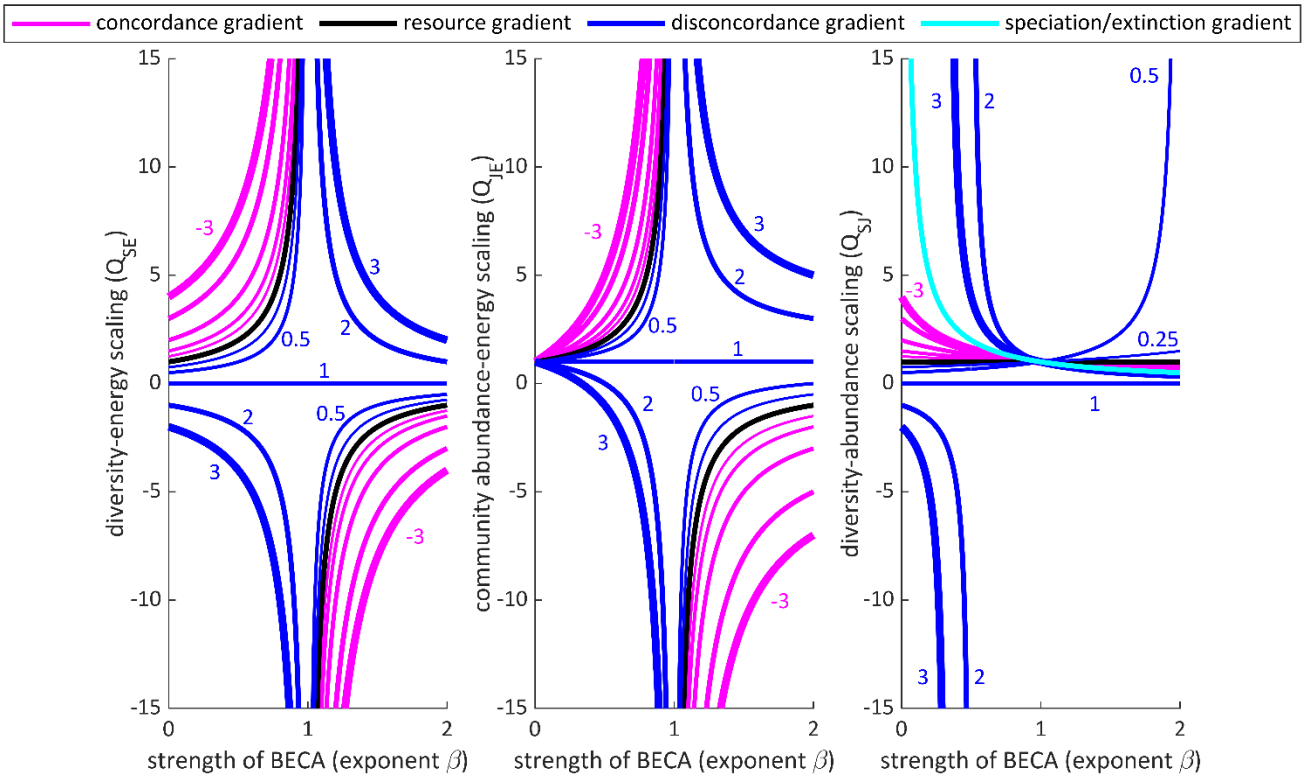

956

957 **Figure 3**. Effects of the J-nullcline on the scaling of species richness and community abundance
958 equilibria along simple and complex environmental gradients. β is the scaling exponent of the J-
959 nullcline quantifying the strength of the effect of diversity on community abundance (BECA). The
960 curves indicate the *S-J-E* scaling exponents for pure speciation/extinction gradients (light blue, r_1 =
961 0), pure resource availability gradients (black, g_1 = 0), and complex gradients in which
962 speciation/extinction and resource availability covary. In a complex gradient, equilibrium mean
963 population size $\widehat{N}$ may decrease with resource availability due to higher speciation or lower
964 extinction in high resource environments (a *concordance gradient*, pink curves, $g_1/r_1 < 0$) or increase
965 with resources (*a discordance gradient*; dark blues curves, $g_1/r_1 > 0$). Thicker curves indicate
966 gradients having larger absolute values of g_1/r_1 (as shown). Note that ETBD predicts all communities
967 have an upper diversity and abundance equilibrium resulting from competition for limited resources
968 ($\beta < 1$) that is stable. If the J-nullcline exhibits facilitation ($\beta > 1$) below this upper stable equilibrium
969 point, then communities can have additional equilibria; however, the equilibria are only stable if

970 they reflect the intersection of the J-nullcline with a second S-nullcline, which occurs when the
971 functions for population size-dependence of speciation and extinction intersect twice (Box 1).
972

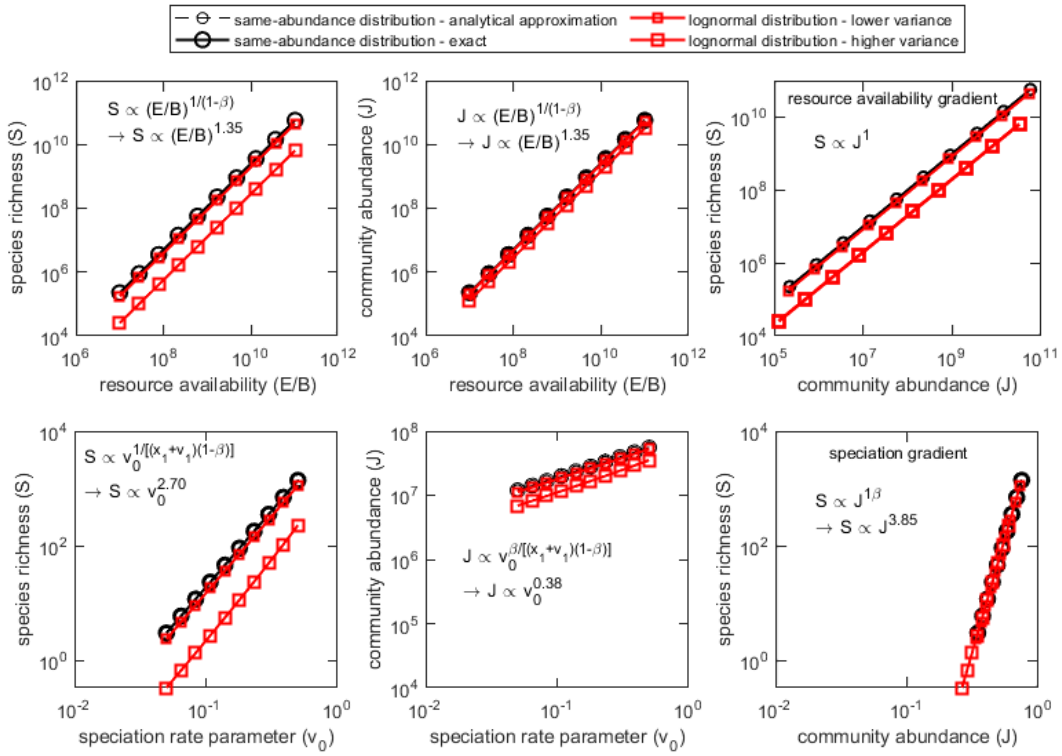

973

974 **Figure 4.** Predicted changes in biodiversity and community abundance along gradients in resource
975 availability (top row) and speciation (bottom row) for different species abundance distributions.
976 Symbols indicate arbitrary locations along the gradient to facilitate comparison between models.
977 Results show that the species abundance distribution has limited effects on the scaling patterns,
978 although it does influence the species richness and community abundance expected for a given set
979 of environmental conditions, and that the analytical power law model accurately approximates the
980 full model (assuming equations 14 and 15). To model communities with lognormal species
981 abundance distributions, the distributions' σ parameter (standard deviation of ln N) was assumed to
982 be either 0.5 or 1.5 for low and high variance species abundance distributions, respectively. The
983 speciation rate parameter (v_0), along with the scaling exponent quantifying the N-dependence of
984 speciation (v_1), determine the proportion of species of a given abundance that speciate within a

given time interval. In all panels, $x_1 = 0.5$, $c = 0.01$, $\beta = 0.26$, $v_1 = 0$. In **A**, **B**, and **C**, $x_0 = 10$, $v_0 = 0.1$. In **D**, **E**, and **F**, $E/B = 10^9$ individuals and $x_0 = 100$.

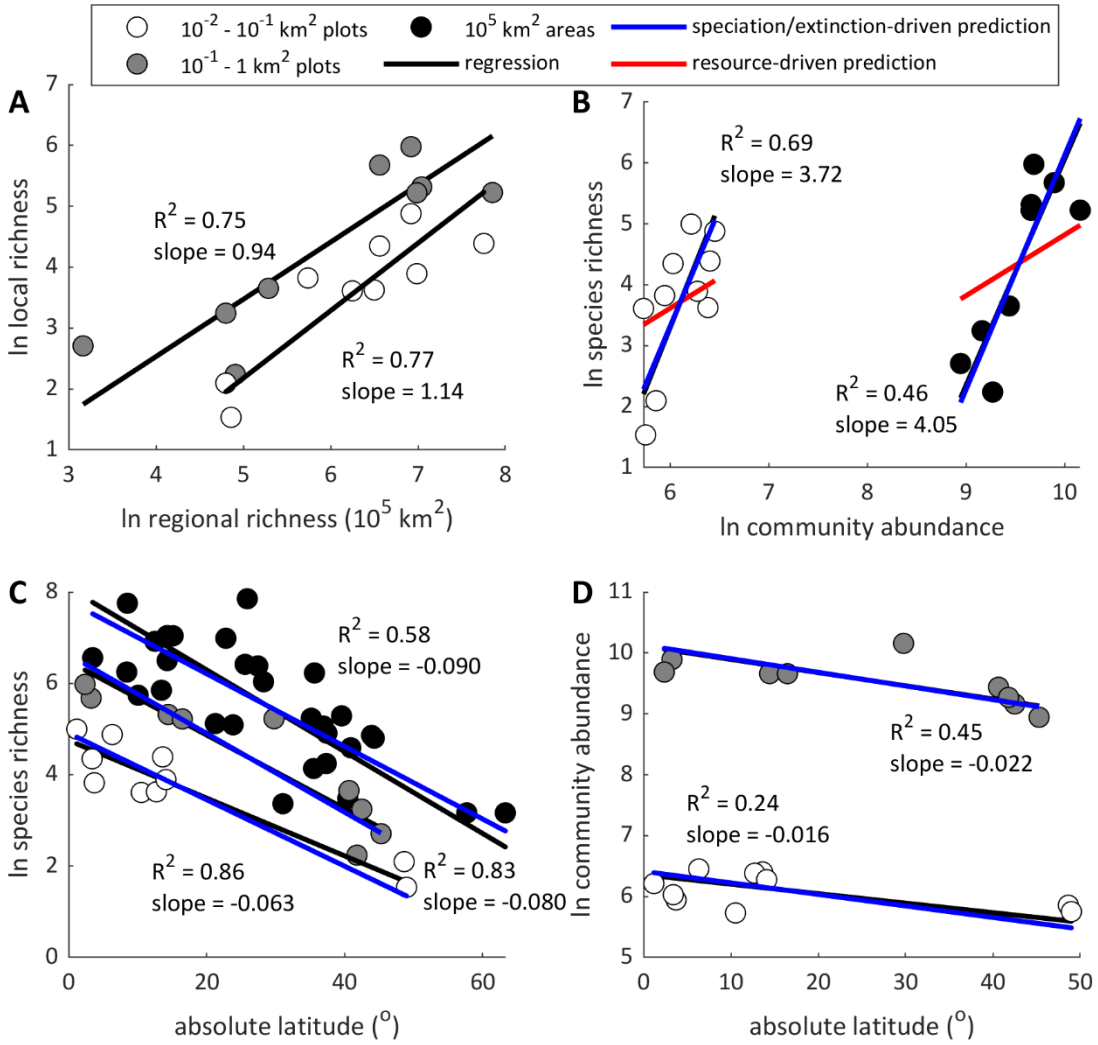

Figure 5. Application of ETBD to among-biome patterns of average tree richness suggests the balance of speciation and extinction, rather than variation in energy availability, is the major driver of their latitudinal diversity gradient. (**A**) Local richness down to 0.01 km^2 grain sizes is proportional to 100,000 km^2 regional richness, indicating that in trees ETBD predictions downscale to these lower grain-sizes without need for amendment. In (**B**), (**C**), and (**D**), the blue lines show the predicted slopes for the relationships between log species richness (S) and log community abundance (J), log species richness and latitude, and log community abundance and latitude assuming a purely speciation/extinction driven gradient ($r_1 = 0$) and $\beta = 0.26$ for the J-nullcline. Predictions are

indistinguishable from the regressions (black lines). Red lines in (**B)** represent the contrasting scenario of a purely resource-driven gradient (i.e. slope of 1 due to $g_1 = 0$). Blue lines in **D** and **E** must assume a value for g_1 (quantifying the degree to which speciation/extinction changes along the gradient), which is estimated from the scaling of log equilibrium mean abundance (ln $\widehat{N}$) with latitude.

Table 1. The main parameters in the core of ETBD, its scaling theory for simple and complex environmental gradients, and its model addressing the effects of extinction, speciation, and the species abundance distribution.

	Description	Symbol
Core	Number of species	S
	Community abundance	J
	Species abundance	N
	Equilibrium species abundance	$\widehat{N}$
Scaling theory	Strength of the biodiversity effect on community abundance (J-nullcline scaling exponent)	β
	Maximum energy supply	E
	Average individual metabolic rate	B
	Environmental gradient	G
	Exponent quantifying the effect of environmental variable G on maximum community abundance ($J_{max} = E/B$)	r_1
	Exponent quantifying the effect of environmental variable G on equilibrium mean species abundance	g_1
Model	Probability that a species of abundance N goes extinct	$P_x(N)$
	Probability that a species of abundance N speciates	$P_v(N)$
	Exponent quantifying dependence of $P_x(N)$ on N	x_1
	Exponent quantifying dependence of $P_v(N)$ on N	v_1
	Coefficient setting the extinction level at a given N	x_0
	Coefficient setting the speciation level at a given N	v_0
	Density function of the species abundance distribution	$f_N(N)$

1008 **Table 2**. Results of the Reduced Major Axis regression analysis at different spatial scales of the
1009 across-biome relationships between absolute latitude, tree species richness (*S*), total number of
1010 individuals (*J*), mean population abundance ($\widehat{N}$) and the comparison of observed slopes to ETDB-
1011 predicted slopes for a speciation/extinction-driven diversity gradient.

Y	X	Grain size (km²)	Predicted Slope	Observed Slope	Lower 95% CI	Upper 95% CI	Intercept	R^2
ln local *S*	ln regional *S*	10^{-1} vs 10^{5} km²		0.940	0.522	1.358	-1.228	0.753
ln local *S*	ln regional *S*	10^{-2} vs 10^{5} km²		1.109	0.621	1.596	-3.366	0.758
ln $\widehat{N}$	latitude	0.1		0.064	0.042	0.085	3.501	0.858
ln $\widehat{N}$	latitude	0.01		0.054	0.039	0.068	1.505	0.893
ln *S*	ln *J*	0.1	3.846	3.720	1.859	5.581	-31.129	0.687
ln *S*	ln *J*	0.01	3.846	4.055	1.634	6.476	-21.031	0.464
ln *S*	latitude	100,000	-0.079	-0.090	-0.112	-0.067	8.085	0.578
ln *S*	latitude	0.1	-0.086	-0.081	-0.110	-0.051	6.481	0.835
ln *S*	latitude	0.01	-0.073	-0.063	-0.083	-0.044	4.752	0.858
ln *J*	latitude	0.1	-0.022	-0.022	-0.036	-0.007	10.110	0.450
ln *J*	latitude	0.01	-0.019	-0.016	-0.027	-0.005	6.358	0.242

1012

1013

Box 1. **Emergence of multiple diversity equilibria and tipping points**. When the speciation and extinction curves have a second intersection point, due to $P_v(N)$ being hump-shaped or $P_x(N)$ being U-shaped, an additional S-nullcline emerges that can lead to additional stable and unstable equilibria. A hump-shape in $P_v(N)$ may arise due to a variety of genetic, geographic, ecological, and evolutionary factors associated with species abundance that could cause a drop in speciation rate in highly abundant species. A U-shaped $P_x(N)$ may arise if large populations have high extinction probabilities due to their susceptibility to epidemics. In such scenarios, the extinction curve slope is greater than the speciation curve slope at the second intersection, leading to the second S-nullcline exhibiting *repulsive* dynamics, such that d*S*/d*t* < 0 for communities to the left of this *repulsive S-nullcline* (blue region in Box Fig. 1B) and d*S*/d*t* > 0 for communities to the right of the repulsive S-nullcline (pink region). Consequently, as shown in Box Figure 1B, if $\beta < 1$ at the *J*-nullcline's intersection with a repulsive S-nullcline, the resulting equilibrium point is unstable, whereas the equilibrium point is stable if $\beta > 1$. When the *J*-nullcline is sigmoidal, the presence of two S-nullclines can thus create a lower stable equilibrium in the accelerating phase of the J-nullcline (where $\beta > 1$) and an unstable equilibrium point (threshold) separating this lower stable equilibrium from the universal upper stable equilibrium (where $\beta < 1$). Tipping points leading to state shifts and hysteresis can occur due to temporary perturbations to the nullclines kicking a community temporarily out of equilibrium into another basin of attraction, the community subsequently being stuck in the alternative stable state even upon returning to initial conditions. Such tipping points could also occur under incremental changes in the height of the *S*-nullclines or *J*-nullcline. Here the system stays in equilibrium up until the bifurcation point, where a small change in conditions shifts the biome to the alternative stable state.

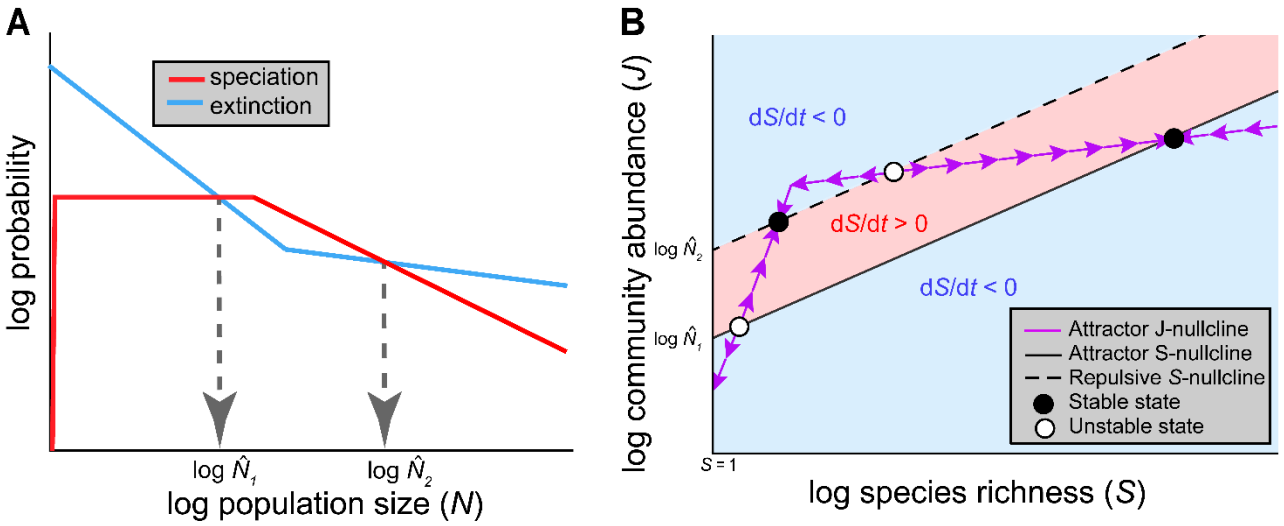

Box 1 Figure 1. Example of how a sigmoidal biodiversity effect on community abundance (J-nullcline) in conjunction with nonlinearities in the origination or extinction curve lead to multiple stable states in biodiversity and community abundance. (**A**) When the speciation curve drops at higher population sizes or the extinction curve increases, there can be two intersections of the curves, leading to potentially two mean population sizes ($\widehat{N}_1$ and $\widehat{N}_2$) for which a community can be at equilibrium. (**B**) These equilibrium mean population sizes determine the heights of the resulting S-nullclines in the log-log S-J phase plane (black lines). A community recovering from a perturbation follows a vertical trajectory to the J-nullcline (purple line) and then follows a trajectory along the J-nullcline indicated by the purple arrows. The direction of this trajectory is determined by whether the community is located in a region in which dS/dt < 0 (blue areas) or dS/dt > 0 (pink area). A sigmoidal J-nullcline is shown (like in Fig. 1C but in log-transformed space), leading to four equilibrium points. In **A**, the speciation curve necessarily drops to zero at non-reproductively viable population sizes, whereas the extinction curve intercepts 1.

Box 2. Integrating ETBD with metabolic theory of ecology (MTE) to predict diversity and abundance along temperature gradients in ectotherms, plants, and microbes. According to MTE, speciation rate should scale as $e^{-E_B/kT}$ due to metabolic rate governing the temperature dependence of genetic divergence rates, giving $P_v = 1 - e^{-v_0 e^{-\frac{E_v}{kT_B}} \Delta t N^{v_1}} \approx v_0 e^{-\frac{E_v}{kT_B}} N^{v_1}$, resource supply rate should scale with temperature as $E = E_0 e^{-E_R/kT_E}$, and metabolic rate should scale as $B = b_0 e^{-E_B/kT_B}$ where E_v, E_R, E_B are the kinetic parameters (effective activation energies) quantifying the temperature dependence of the rates, *k* is Boltzmann's constant in electron volts, v_0, E_0, and b_0 are normalization coefficients, and T_B and T_E are body and ecosystem temperatures, respectively, in kelvin. MTE assumes $E_v = E_B$ and $T_B \approx T_E$ in ectotherms. Both MTE and neutral biodiversity theory implicitly assume $v_1 \approx 1$, as they model speciation as a per capita process (Allen et al. 2006; Allen and Savage 2007). We do not make this strong assumption, as it has limited theoretical or empirical support and models of speciation suggest the N-dependence is more complex in real populations (Gavrilets 2003). Thus, assuming the same-abundance species distribution we obtain $S \propto e^{E_B - E_R - E_v(x_1+v_1)/kT(1-\beta)}$ and $J \propto e^{E_B - E_R - \beta E_v(x_1+v_1)/kT(1-\beta)}$. Adopting MTE's previously implicit assumption that $E_R = E_B$, such that E/B is independent of temperature, we obtain

$$S \propto e^{-E_v(x_1+v_1)/kT(1-\beta)} \quad (1)$$

$$J \propto e^{-\beta E_v(x_1+v_1)/kT(1-\beta)} \quad (2)$$

And

$$\widehat{N} = \left(\frac{x_0}{v_0} e^{E_v/kT}\right)^{\frac{1}{x_1+v_1}} \quad (3)$$

These equations show that the population size-dependence of extinction and speciation, along with the biodiversity effect on community abundance (quantified by β), affect the temperature dependence of diversity. This contrasts with MTE's prediction that $\hat{J}$ is invariant of temperature and

$\hat{S} \propto e^{\frac{-0.65}{kT}}$ due to the temperature dependence of richness in plants and ectotherms solely reflecting the temperature dependence of rates of speciation or interspecific interactions (Allen et al. 2002; Brown et al. 2004). The MTE predictions fall well outside the 95% Confidence Intervals in trees (Table S2). Using equation 3 and assuming E_v = 0.65 eV (Allen et al. 2006), we calculate from our tree analysis that $x_1 + v_1 = 0.70$ in trees, leading to the predictions from equations 1 and 2 of $S \propto e^{-0.61/kT}$ and $J \propto e^{-0.16/kT}$, which also deviates from the observed scaling relationships (Table S2). This indicates that other parameters of extinction (x_0 or x_1) or speciation (v_1) are varying along the thermal gradient or that speciation depends on temperature differently than expected from MTE, pointing to the need for more research on these dependencies, as well the usefulness of applying our generalized scaling approach to the study of complex gradients.

Supplementary Materials for

The equilibrium theory of biodiversity dynamics: a general framework for scaling species richness and community abundance along environmental gradients

Jordan G. Okie*, David Storch

*Corresponding author. Email: Jordan.Okie@asu.edu

This file includes:

Supplementary Text

Emergence and Properties of the S-nullcline

Consider that at equilibrium, the total rate of extinction $X_{TOT} = S\int_0^\infty P_x(N)f_N(N,\widehat{N})dN$ must be equal to the total rate of speciation $V_{TOT} = S\int_0^\infty P_v(N)f_N(N,\widehat{N})dN$, giving

$$\int_0^\infty P_x(N)f_N(N,\widehat{N})dN = \int_0^\infty P_v(N)f_N(N,\widehat{N})dN \quad \text{(S1)}$$

Where $P_x(N)$ and $P_v(N)$ are the functions characterizing the dependence of extinction and speciation probability, respectively, on population size, $f_N(N,\widehat{N})$ is the probability density function of the species abundance distribution, and $\widehat{N}$ is equilibrium mean species abundance.

A feature of the species abundance distribution (SAD) is that it must have a mathematically defined mean species abundance, in which case $f_N(N)$ can be considered a function of mean abundance. Often a probability density function has a parameter directly equivalent or related to the mean (as in the normal distribution), simplifying the mathematics, but it is not a requirement of the theory. Since $\widehat{N}= J/S$, we write the SAD density function as $f_N(N,\widehat{N})$, highlighting the fact that the equilibrium distribution is necessarily tied to the ratio of *J* to *S*. Put another way, we assume the SAD has one free parameter that affects $\widehat{N}$, the value of which is set by the ratio of *J* to *S* at equilibrium, which, as we shall see, is determined by the balance of extinction and speciation modulated by the SAD. The SAD may also have shape or scale parameters (e.g., a variance parameter in the lognormal distribution) required to uniquely define the distribution, which are assumed here to be intrinsic properties of the assembly dynamics and so input parameters to ETDB. For baseline theory and modeling, we make the null assumption that all such input parameters, should they exist, are independent of *S* and *J*.

Eq. S1 implies that $\widehat{N}$ is some implicit or explicit function W of system parameters: $\widehat{N} = J/\hat{S} = W(v_0, x_0, \ldots)$, where $\hat{S}$ denotes S when $\mathrm{d}S/\mathrm{d}t = 0$ and inputs to W are the two or more parameters of $P_x(N)$ and $P_v(N)$ (denoted as x_i and v_i, respectively) and parameters n_i, should they

exist, of the species abundance distribution. Rearranging $\frac{J}{\hat{S}} = W(v_i,\ x_i, \dots)$, it follows that the S-nullclines are linear with a slope determined by W:

$$\hat{S} = J/W(v_i,\ \varepsilon_i, \dots) \quad \text{(S2a)}$$

or

$$J = W(v_i,\ \varepsilon_i, \dots)\hat{S} \quad \text{(S2b)}$$

If $P_x(N)$ and $P_v(N)$ intersect more than once, there is more than one equilibrium $\widehat{N}$ and so more than one S-nullcline (Box 1). However, for typical extinction and speciation functions, there are only one or two intersections. Additional intersections of the speciation and extinction curves at large scales and across a variety of biota resulting from more complicated functions for P_v and P_x seem unlikely, requiring an assumption of more idiosyncratic eco-evolutionary associations. Thus, here we only consider the baseline expectation that there are one or two S-nullclines.

Note that the existence of a diversity equilibrium requires that $P_x(N)$ and $P_v(N)$ intersect at a positive abundance, because otherwise communities can never have a positive equilibrium richness since speciation would be greater than extinction across all abundance classes or vice versa. Similarly, f_N must be able to be sufficiently positive both over some range of N where $P_x(N) \geq P_v(N)$ and where $P_x(N) < P_v(N)$ so that there exists a mean abundance that allows $X_{TOT} = V_{TOT}$. For instance, if the assumed SAD function has an upper tail cutoff point (that is, $f_N(N > N_{max}) = 0$), at abundance N_{max} less than the intersection of the extinction and origination curves (assuming they only intersect once) then the system could never achieve an equilibrium. It's also worth noting that if $P_v(N)$ and $P_x(N)$ are identical, any mean abundance allows for $\mathrm{d}S/\mathrm{d}t = 0$ and the function W does not exist; however, due to the contrasting mechanics of speciation and extinction, this scenario is impossible, since at low N, extinction probability is bound to be very high, approaching 1, whereas speciation probability is much lower than 1.

To understand the S-nullcline behavior, consider the idealized scenario in which all species have the same abundance—the "same-abundance distribution". Solving Eq. S1 using same-

abundance distribution (i.e., a Dirac delta function), it follows that $\widehat{N}$ occurs at the intersection point $\dot{N}$ of $P_v(N)$ and $P_x(N)$. Departures from the same-abundance SAD push $\widehat{N}$ away from $\dot{N}$, generally to larger values, but $\dot{N}$ is the main determinant of $\widehat{N}$. $P_v(N)$ and $P_x(N)$ affect the S and J-dependence of X_{TOT} and V_{TOT}, determining when attractor ("stabilizing") or repulsive ("destabilizing") dynamics around the S-nullcline are expected. Specifically, the slopes at $\dot{N}$ determine whether or not the associated S-nullcline is repulsive or an attractor—that is, whether or not following deviations from $\widehat{N}$, changes in S eventually return N to $\widehat{N}$ (*attractor S-nullcline*) or push N further from $\widehat{N}$ (*repulsive S-nullcline*). For the same-abundance SAD, if $\frac{dP_x(\dot{N})}{dN}<\frac{dP_v(\dot{N})}{dN}$, then the S-isocline exhibits attractor dynamics; whereas if $\frac{dP_x(\dot{N})}{dN}>\frac{dP_v(\dot{N})}{dN}$, then repulsive dynamics are exhibited.

Notes on the Species Abundance Distribution

To address the effects of the species abundance distribution, we have treated species abundance N as a continuous variable, as unless community abundance J is exceedingly small, use of a probability density function to characterize the species abundance distribution can work well as a continuous approximation of a discrete variable.

We assume that following any perturbation to an equilibrium state, the species abundance distribution recovers to the original function $f_N(N)$ by the end of the time interval, although its mean may change if the community's diversity or abundance is out of equilibrium. In other words, we assume that the ecological and statistical mechanisms of community assembly and population dynamics act to re-equilibrate the SAD (Pueyo et al. 2007). This is a reasonable baseline assumption, given that if it were broken, the SAD could diverge to an extreme distribution unless some other mechanisms were invoked to stabilize it into some other form. In several existing ecological theories this continual re-equilibration of the SAD is implicitly assumed or it is the result of modeled population dynamics, such as in the neutral theory of biodiversity (Hubbell 2001). However, we have not assumed any constraints on the population dynamics of individual species, only that the results of

the ensemble of dynamics follows our functions for extinction, speciation, and the SAD. We do not assume that communities far from equilibrium have SADs identical to $f_N(N)$; however, if their SADs differ, we assume that biodiversity dynamics driven by differences between extinction and origination are the dominant drivers of dS/dt. This assumption is warranted, at least for making coarse-grained predictions of equilibrium stability and diversity trajectories, as we show in Figure 4 that the SAD has a minimal effect on biodiversity patterns (compared to other variables).

On general features of $P_v(N)$ and $P_x(N)$

It is worth noting there are some fundamental biological constraints to $P_x(N)$ and $P_v(N)$ that could be important when modeling particular scenarios involving hyper-rich communities or communities with very small abundances. For asexually reproducing taxa, $P_v(N < 1) = 0$ and $P_x(N < 1) = 1$, whereas for sexually reproducing taxa, $P_v(N < 2) = 0$ and $P_x(N < 2) = 1$ (since a couple is required for sexual reproduction). However, since generally $\widehat{N} \gg 2$ (e.g., in the tree data, it's $\widehat{N} \approx 10^8$ individuals in 10^5 km^2), these constraints are of limited importance for general biodiversity patterns.

Some coarse-grained features of the extinction and speciation curves can be deduced in order to shed light on the determinants of the intersection of curves. Extinction probability generally decreases with N due to the reduced effects of demographic and environmental stochasticity on large populations and the detrimental effects of genetic drift in small populations (Rosenzweig 1995; Ovaskainen and Meerson 2010). Extinction probability may, however, stop decreasing or even increase at very large population sizes due to large-scale perturbations that wipe out entire populations, regardless of their size. For example, large populations could be susceptible to epidemics due to infectious diseases being positively population-size dependent.

In contrast, speciation probability may increase or decrease with population size, depending on the geographic template and characteristics of the biota (e.g., traits increasing the chances of allopatric or sympatric speciation). At very low N, a population necessarily has a low probability of speciation for both genetic and geographic reasons (Rosenzweig 2001; Gavrilets 2003), whereas the

population necessarily has a high probability of extinction. However, unless the biota is on an evolutionary path to full extinction, the speciation curve must be higher than the extinction curve at some larger values of *N*, thereby intersecting the extinction curve and having a higher slope (less negative or positive) than the extinction curve at their intersection. Past this intersection point, with increasing *N*, the speciation curve may: (1) continue to increase with *N*, due to covarying organism traits and geographic factors contributing to speciation likelihood or the per capita probability of speciation being invariant of population size, as in the neutral theory of biodiversity, which implies $P_v(N) \sim N^1$ (Allen and Savage 2007); (2) be relatively invariant of *N*; or (3) eventually decrease with *N* and possibly intersect $P_x(N)$ again–e.g., if more abundant, wide-ranging species tend to be generalists and better dispersers and so less sensitive to geographic barriers (Gaston and Chown 1999; Jablonski and Roy 2003). Additional intersections of the curves, although theoretically possible, are unlikely, especially at large scales and across a variety of biomes and biota.

Derivations of $P_v(N)$ and $P_x(N)$

We derive a baseline function for $P_x(N)$ by assuming two general results of stochastic extinction theory that are predicted by a variety of models (Ovaskainen and Meerson 2010): (1) population/species extinction times t_x follow an exponential distribution with the probability density function $f_x(t_x) = (\frac{1}{T})e^{-(\frac{1}{T})t_x}$, where T is the mean time to extinction; (2) when the effects of environmental stochasticity dominates over demographic stochasticity (as expected over biogeographic scales), environmental stochasticity generally leads to *T* exhibiting power law behavior when the population size carrying capacity K >>1, such that $T \sim K^{x_1}$, where x_1 is the scaling exponent (Ovaskainen and Meerson 2010). Since generally $N \sim K$ for $K >> 1$ (Ovaskainen and Meerson 2010), we can assume $T = {x_0}^{-1} N^{x_1}$, where x_0 is a prefactor, with larger values leading to decreased times to extinction. Consequently, the proportion of species of abundance *N* that go extinct

within the time interval Δt is determined by substituting $T = {x_0}^{-1}N^{x_1}$ into $f_x(t_x) = (\frac{1}{T})e^{-(\frac{1}{T})t_x}$ and integrating over Δt (i.e., $P_x(N) = \int_0^{\Delta t} x_0 N^{-x_1} e^{-x_0 N^{-x_1} t_x} dt_x$), giving

$$P_x(N) = 1 - e^{-x_0 \Delta t N^{-x_1}} \quad \text{(S3)}$$

Since we have integrated over the probability density function $f_x(t_x)$, $P_x(N)$ may be interpreted as the probability that a species of abundance *N* goes extinct in the time interval. Although equation S3 is expected to only rigorously apply to *N*>>1, prediction error at low *N* should be marginal, given that all stochastic extinction models predict high probabilities of extinction at low *N*.

For $x_1 > 0$, as $N \to \infty$ or $\Delta t \to 0$, Equation S3 follows exactly a power law with scaling exponent x_1, which can be derived by substituting in $e^y = N$ and solving for $d(log\ P_x)/dy$ in the limits of $N \to \infty$ or $\Delta t \to 0$. The prefactor *b* for this power law (bN^{-x_1}) can similarly be derived by using l'Hopital's Rule to solve for *b* in the limit $N \to \infty$ at the intersection of Equation S3 and bN^{-x_1}, i.e., $b = \lim_{N\to\infty}(1 - e^{-x_0 N^{-x_1}\Delta t})N^{x_1}$, which gives $b = \Delta t x_0$. Note that at very small *N* (the exact values of which depends on Δt), the power function overestimates $P_x(N)$ compared to Equation S3 and can become improper (predicting P_x>1 at $N < N_{crit}$). However, since Δt can be made arbitrarily small in our theory, the power law can provide a very accurate approximation for $N > N_{crit}$, and for $N < N_{crit}$, $P_x(N) \approx 1$ with reasonably low error. So, in sum, Eq S3 is very well approximated by a power law, which it converges exactly to for $N \to \infty$ or $x_0 \Delta t \to 0$, giving

$$P_x(N) \approx \Delta t x_0 N^{-x_1}. \quad \text{(S4)}$$

Use of such a power law can help facilitate development of analytical predictions and heuristic understanding. We verified that using Equation S4 provides nearly identical results regarding the relationships between variables (such as *S* and *J*) to Equation S3 for a range of ecologically and evolutionary relevant parameter values (Figure 3 and Figure S1).

Developing baseline theory for speciation rate's dependence on *N* is less straightforward, as there's much more limited theoretical understanding of it. An integrative consideration of population genetics, biogeography, and evolutionary ecology suggests that population size and its correlates

could have both positive and negative effects on rates of speciation. For instance, large populations tend to have large geographic ranges, which could increase the chance that a population is separated by a geographic barrier that leads to allopatric speciation (Rosenzweig 1995; Smyčka et al. 2023). Similarly, higher *N* could increase the chance that an individual is born with a mutation that leads to sympatric speciation or a trait that allows the individual to occupy a new niche or area. On the other hand, species with small *N* may tend to have certain traits (such as being ecological specialists), that may make them more likely to speciate. For example, if they are obligate mutualists (like pollinators feeding on nectar) or parasites then there may be forces to coevolve with their hosts--the host speciating eventually leading to the pollinator or parasites co-speciating as the populations coevolve with the new host species (diversity begetting diversity).

Given the uncertainty, complexity, and idiosyncrasy surrounding the speciation process, we adopt a scaling approach identical to our approach to extinction, such that $T = {v_0}^{-1}N^{v_1}$, where v_0 is a prefactor, with larger values leading to decreased mean times to speciation (and thus increased mean probabilities of speciation). This gives $P_v(N) = 1 - e^{-v_0 \Delta t N^{v_1}}$ and thus the scaling approximation

$$P_v(N) \approx \Delta t v_0 N^{v_1} \quad \text{(S5)}$$

Equation S5 can capture the scenario in which the balance of positive and negative effects of *N* on speciation lead to speciation rate increasing or decreasing with *N*. It can be used to address idealized expectations for speciation, including the scenario in which speciation is independent of *N* (i.e., $v_1 = 0$) and the scenario in which speciation rate increases linearly with *N* (i.e., $v_1 = 1$), due to speciation being considered a neutral per capita process, as in the neutral theory of biodiversity (Allen and Savage 2007).

References

Allen, A. P., and V. M. Savage. 2007. Setting the absolute tempo of biodiversity dynamics. Ecology letters 10:637–646.

1284 Gaston, K. J., and S. L. Chown. 1999. Geographic range size and speciation. Evolution of biological
1285 diversity 236–259.
1286 Gavrilets, S. 2003. Perspective: models of speciation: what have we learned in 40 years? Evolution
1287 57:2197–2215.
1288 Hubbell, S. P. 2001. The unified neutral theory of biodiversity and biogeography Princeton
1289 University Press. Princeton, New Jersey, USA.
1290 Jablonski, D., and K. Roy. 2003. Geographical range and speciation in fossil and living molluscs.
1291 Proceedings of the Royal Society of London. Series B: Biological Sciences 270:401–406.
1292 Ovaskainen, O., and B. Meerson. 2010. Stochastic models of population extinction. Trends in
1293 ecology & evolution 25:643–652.
1294 Rosenzweig, M. L. 1995. Species diversity in space and time. Cambridge Univ Pr.
1295 Rosenzweig, M. L. 2001. Loss of speciation rate will impoverish future diversity. Proceedings of the
1296 National Academy of Sciences 98:5404–5410.
1297 Smyčka, J., A. Toszogyova, and D. Storch. 2023. The relationship between geographic range size
1298 and rates of species diversification. Nature Communications 14:5559.
1299
1300

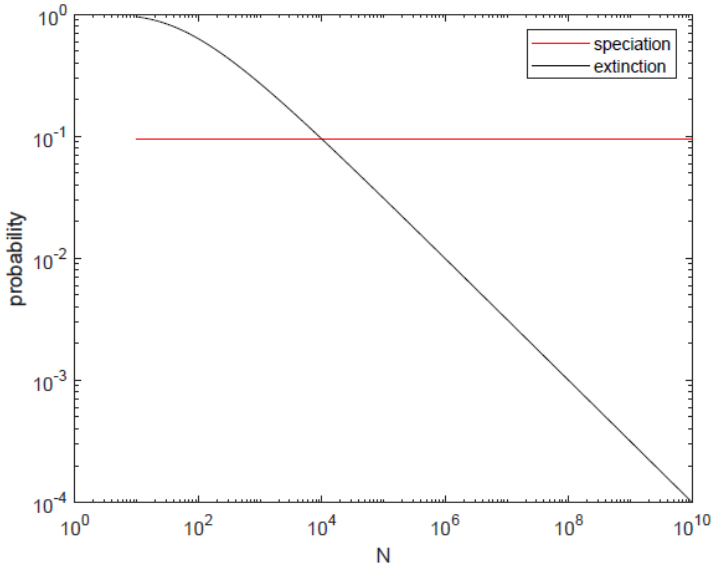

1301

Figure S1. Illustration of the population size-dependence of probabilities of extinction and speciation with the exponent parameters assumed for the full models shown in Figure 4. Because the curves are straight at and near their intersection, the power law approximation works well to model gradients in equilibrium diversity and abundance. Here the speciation probability was assumed to be independent of N (that is, $v_1 = 0$). The plotted speciation curve extends to $N = 1$, but it becomes numerically more intensive to plot with the full model, so was not shown here.

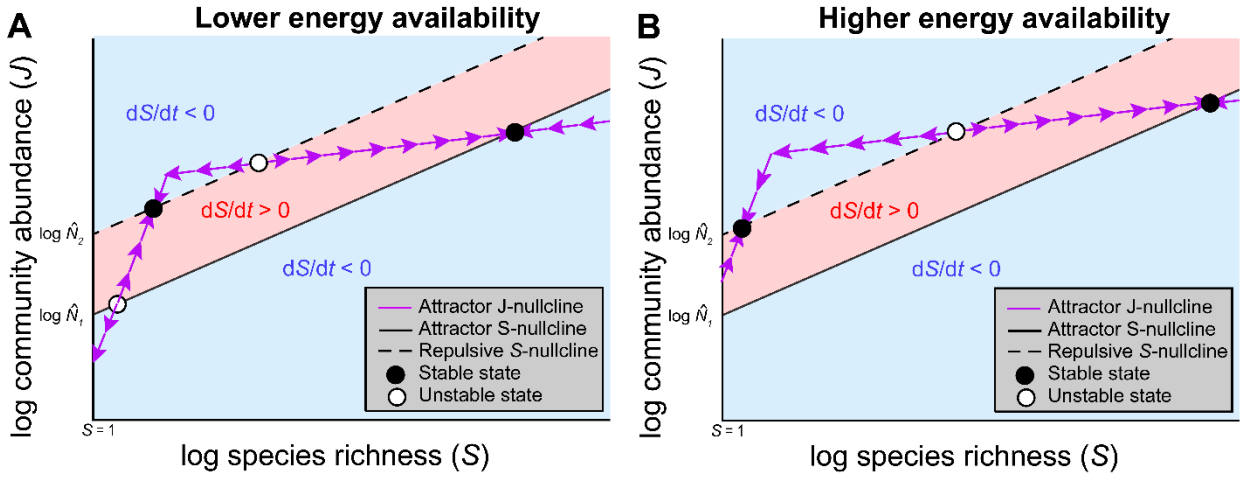

Figure S2. Illustration of how an increase in the height of the J-nullcline differentially influences the species richness and community abundance of equilibrium points, depending on the scaling of the J-nullcline around the equilibrium point. Increased energy availability *(E)*, reduced individual metabolic rate *(B)*, or an increase in the ability of communities of a given S to use available resources (c) increases the height of the J-nullcline, as shown in **B**. When the J-nullcline is steeper than the S-nullcline around the equilibrium point (i.e., if $\beta > 1$ due to facilitation), the unstable and stable equilibrium point's S and J decreases, as shown in **B.** If the J-nullcline height is sufficiently increased, these equilibrium points may even disappear, due to the facilitation-phase of the J-nullcline no longer intersecting the S-nullclines. In contrast, an increase in the height of the J-nullcline leads to an increase in the S and J of the stable equilibrium point found at the intersection with the attractor S-nullcline, as well as an increase in the S and J of the unstable equilibrium point found at the intersection with the repulsive S-nullcline.

Table S1. Results of the Reduced Major Axis regression analysis using country-level species richness as a measure of regional species richness (i.e., without standardizing to 100,000 km^2).

Y	X	Observed Slope	Lower 95% CI	Upper 95% CI	Intercept	R^2
ln regional S	absolute latitude	-0.085	-0.095	-0.074	8.524	0.43
ln local S (per 0.1 km^2)	ln regional S	1.111	0.615	1.607	-2.984	0.75
ln local S (per 0.01 km^2)	ln regional S	1.08	0.707	1.454	-3.518	0.79

Table S2. Results of the Reduced Major Axis regression analysis of inverse mean annual air temperature (1/kT, where k is Boltzmann's constant in eV and T is temperature in kelvins), log species richness (S), log total number of individuals (J), log mean population abundance ($\widehat{N}$) in trees from terrestrial biomes.

Y	X	Observed Slope ("Activation Energy")	Lower 95% CI	Upper 95% CI	Intercept	R^2	Area (km^2)
ln S	$1/kT$	-1.234	-1.771	-0.697	54.106	0.763	0.1
ln S	$1/kT$	-1.041	-1.377	-0.704	44.765	0.843	0.01
ln $\widehat{N}$	$1/kT$	0.977	0.573	1.381	-34.201	0.786	0.1
ln $\widehat{N}$	$1/kT$	0.886	0.569	1.203	-32.562	0.807	0.01
ln J	$1/kT$	-0.332	-0.560	-0.104	22.912	0.408	0.1
ln J	$1/kT$	-0.257	-0.421	-0.093	16.226	0.385	0.01

1332 **Table S3.** Calculated/estimated mean tree species richness and community abundance of different
1333 biomes and biogeographic realms at spatial grains ranging from 0.01 km^2 to 100,000 km^2.

Scale (km^2)	Habitat-realm combination	Counts	Mean log_{10} species richness	Mean log_{10} community abundance	Mean annual temperature (°C)	Mean latitude (°)
100000	Boreal Forests/Taiga_Nearctic	1	1.375	NA	-7.059	57.715
100000	Boreal Forests/Taiga_Palearctic	4	1.375	NA	-0.406	63.304
100000	Deserts and Xeric Shrublands_Afrotropic	4	2.224	NA	21.478	21.268
100000	Deserts and Xeric Shrublands_Australasia	1	2.787	NA	21.458	25.574
100000	Deserts and Xeric Shrublands_Nearctic	5	2.201	NA	11.375	36.906
100000	Deserts and Xeric Shrublands_Neotropic	7	2.714	NA	24.488	8.424
100000	Deserts and Xeric Shrublands_Palearctic	20	1.462	NA	18.844	31.057
100000	Flooded Grasslands and Savannas_Afrotropic	1	2.541	NA	21.223	13.453
100000	Mediterranean Forests, Woodlands and Scrub_Neotropic	1	1.797	NA	8.646	35.513
100000	Mediterranean Forests, Woodlands and Scrub_Palearctic	9	1.844	NA	15.131	37.344
100000	Montane Grasslands and Shrublands_Afrotropic	3	2.212	NA	19.175	23.833
100000	Montane Grasslands and Shrublands_Palearctic	4	2.705	NA	2.198	35.633
100000	Temperate Broadleaf and Mixed Forests_Nearctic	24	2.297	NA	10.757	39.567
100000	Temperate Broadleaf and Mixed Forests_Palearctic	38	2.085	NA	8.902	44.296
100000	Temperate Conifer Forests_Indo-Malay	1	2.772	NA	10.254	27.416
100000	Temperate Conifer Forests_Nearctic	9	2.132	NA	11.992	37.441
100000	Temperate Conifer Forests_Palearctic	5	2.111	NA	7.122	43.913
100000	Temperate Grasslands, Savannas and Shrublands_Nearctic	9	1.994	NA	10.198	40.904
100000	Temperate Grasslands, Savannas and Shrublands_Neotropic	1	2.275	NA	14.200	35.178
100000	Temperate Grasslands, Savannas and Shrublands_Palearctic	4	1.511	NA	5.282	40.460
100000	Tropical and Subtropical Coniferous Forests_Indomalay	1	2.621	NA	14.053	28.253
100000	Tropical and Subtropical Coniferous Forests_Neotropic	2	3.060	NA	24.002	14.277

100000	Tropical and Subtropical Dry Broadleaf Forests_Indomalay	1	3.059	NA	26.121	15.145
100000	Tropical and Subtropical Dry Broadleaf Forests_Neotropic	1	3.368	NA	25.008	8.514
100000	Tropical and Subtropical Grasslands, Savannas and Shrublands_Afrotropic	27	2.493	NA	24.901	10.079
100000	Tropical and Subtropical Grasslands, Savannas and Shrublands_Neotropic	12	2.823	NA	23.602	14.275
100000	Tropical and Subtropical Moist Broadleaf Forests_Afrotropic	6	2.850	NA	24.606	3.482
100000	Tropical and Subtropical Moist Broadleaf Forests_Indomalay	12	3.035	NA	21.312	22.793
100000	Tropical and Subtropical Moist Broadleaf Forests_Neotropic	22	3.006	NA	23.277	12.519
100000	Tropical and Subtropical Moist Broadleaf Forests_Palearctic	2	3.411	NA	15.457	25.896
0.1	Boreal Forests/Taiga_Nearctic	1	1.176	3.884	4.200	45.290
0.1	Temperate Broadleaf and Mixed Forests_Nearctic	4	1.586	4.098	10.000	40.640
0.1	Temperate Broadleaf and Mixed Forests_Palearctic	5	1.409	3.979	7.640	42.502
0.1	Temperate Conifer Forests_Nearctic	2	0.972	4.026	8.450	41.790
0.1	Tropical and Subtropical Dry Broadleaf Forests_Indomalay	1	2.310	4.195	23.600	14.430
0.1	Tropical and Subtropical Moist Broadleaf Forests_Afrotropic	2	2.466	4.296	24.700	3.255
0.1	Tropical and Subtropical Moist Broadleaf Forests_Indomalay	10	2.268	4.195	22.010	16.473
0.1	Tropical and Subtropical Moist Broadleaf Forests_Neotropic	3	2.596	4.207	22.667	2.373
0.1	Tropical and Subtropical Moist Broadleaf Forests_Palearctic	1	2.270	4.411	11.100	29.770
0.01	Deserts and Xeric Shrublands_Neotropic	1	1.568	2.489	23.600	10.530
0.01	Mangroves_Neotropic	1	2.170	2.698	26.200	1.180
0.01	Temperate Broadleaf and Mixed Forests_Palearctic	3	0.911	2.544	7.900	48.639
0.01	Temperate Conifer Forests_Palearctic	14	0.667	2.498	5.500	48.990
0.01	Tropical and Subtropical Dry Broadleaf Forests_Neotropic	14	1.906	2.781	23.700	13.629
0.01	Tropical and Subtropical Grasslands, Savannas and Shrublands_Afrotropic	31	1.660	2.581	24.377	3.720
0.01	Tropical and Subtropical Grasslands, Savannas and Shrublands_Neotropic	22	1.575	2.772	26.109	12.720
0.01	Tropical and Subtropical Moist Broadleaf Forests_Afrotropic	103	1.888	2.619	24.730	3.404
0.01	Tropical and Subtropical Moist Broadleaf Forests_Indomalay	107	1.691	2.726	24.537	14.101
0.01	Tropical and Subtropical Moist Broadleaf Forests_Neotropic	177	2.119	2.802	25.759	6.321

1334